Earth Syst. Sci. Data, 18, 8167–8189, 2026
https://doi.org/10.5194/essd-18-8167-2026
© Author(s) 2026. This work is distributed under
the Creative Commons Attribution 4.0 License.

Open Access Earth System Science Data

Climatology of the sea temperature from long-term in situ observations: Northern Chilean Patagonia

Cécile Pujol[1], Alexander Barth[1], Iván Pérez-Santos[2,3], Pamela Linford[3], and Aida Alvera-Azcárate[1]

[1]GeoHydrodynamics and Environment Research, University of Liège, Liège, Belgium
[2]Centro de investigación i~mar, Universidad de Los Lagos, Puerto Montt, Chile
[3]Centro de Investigación Oceanográfica en el Pacífico Sur-Oriental COPAS COASTAL, Departamento de Oceanografía, Universidad de Concepción, Concepción, Chile

Correspondence: Cécile Pujol (cecile.pujol@uliege.be)

Received: 16 January 2026 – Discussion started: 18 February 2026
Revised: 16 August 2026 – Accepted: 11 September 2026 – Published: 9 November 2026

Abstract. Ocean climatologies are essential for understanding the mean state and variability of marine systems, providing reference conditions for detecting anomalies, assessing ecosystem functioning and identifying long-term trends. In this study, we present the first high-resolution, four-dimensional temperature climatology for Northern Chilean Patagonia, a region characterised by the presence of a complex network of fjords and channels. The climatology was generated from approximately three million in situ observations collected over the past 75 years from multiple datasets. Using the Data Interpolating Variational Analysis in *n* dimensions (DIVAnd) tool, temperature fields were reconstructed with a horizontal resolution of about 900 m and over 32 vertical levels, producing monthly fields from the surface to 400 m depth. The resulting climatology accurately reproduces the main spatial and seasonal temperature patterns reported in previous studies. Surface temperatures show strong summer gradients between the open Pacific and Northern Patagonia, while enclosed regions such as Reloncaví Sound, Comau and Puyuhuapi Fjords exhibit pronounced seasonal amplitude compared with more stable basins such as Corcovado Gulf. Below surface, temperature gradients become smoother and the thermocline deepens in summer, typically ranging between 10 and 50 m. At 100 m depth, temperatures are relatively constant throughout the year, but spatial variations are still observed, with Ancud Gulf and Reloncaví Sound being slightly warmer. In addition, a daily-derived climatology for the upper 100 m (14 depth levels) was generated from the monthly fields using temporal interpolation and smoothing, in order to support applications requiring daily temporal resolution. These temperature climatologies provide a refined and physically consistent representation of the oceanographic structures of Northern Patagonia, offering an essential baseline for future modelling, monitoring and climate-change assessments in a region where satellite observations are limited by persistent cloud cover and complex topography. All climatologies generated in this study are freely available online as NetCDF3-Classic datasets (https://doi.org/10.5281/zenodo.21959707, Pujol et al., 2026).

1 Introduction

Ocean climatologies are fundamental tools for understanding and characterising the mean state of the ocean and its long-term variability. They provide reference conditions for a given period that enable the calculation of anomalies, the assessment of ecosystem functioning and the detection of trends associated with climate change (Cheng and Zhu, 2015; Goebeler et al., 2022; Shahzadi et al., 2021b). By offering a consistent baseline against which current or future observations can be compared, climatologies allow scientists to identify whether current or future conditions are normal, anomalous or changing over time (e.g. Cheng and Zhu, 2015; Flaounas et al., 2022; Hobday et al., 2016; Martínez-Moreno et al., 2022). Climatological products derived from a wide range of physical and biogeochemical parameters are also

essential for calibrating and validating numerical models, as well as for supporting the sustainable management of marine resources (Barnier et al., 1995; Bianchi et al., 2021; Brodie et al., 2023; Senay et al., 2023). These products are typically constructed over multi-decadal periods to represent the mean conditions of a specified reference period. In oceanographic and atmospheric sciences, a minimum of 30 years of data is generally recommended to ensure that climatologies capture the influence of long-term climate variability, including large-scale processes such as the El Niño Southern Oscillation (WMO, 2023).

Ocean climatological products can be generated from satellite observations, numerical models, in situ measurements obtained from ship-based profiles, moorings and autonomous platforms, or from reanalysis products that combine these diverse data sources (Embury et al., 2023; European Union-Copernicus Marine Service, 2018; Huang et al., 2021; Simoncelli et al., 2020). Each approach offers distinct advantages: the increasing availability of high-resolution satellite data has substantially improved the spatial and temporal coverage of coastal observations, however, in situ measurements remain indispensable for subsurface characterisation of the ocean state and for model and satellite data calibration and validation (Dickey et al., 2006; Legler et al., 2015; Minnett et al., 2019).

Chilean Patagonia, located in the southern part of Chile (41-56° S), is a highly complex and dynamic coastal region. It is characterised by an extensive network of fjords and channels, strong freshwater inputs from rivers and glaciers that generate sharp salinity gradients and highly variable bathymetry (Narváez et al., 2019; Strub et al., 2019; Vásquez et al., 2021). These systems are strongly influenced by both oceanic processes from the Pacific Ocean and terrestrial freshwater discharge, resulting in marked spatial heterogeneity (Narváez et al., 2019; Saldías et al., 2021; Strub et al., 2019). In recent decades, Northern Patagonia (41–47° S) has received growing scientific attention, partly driven by the rapid expansion of aquaculture and its ecological implications (FAO, 2024; Subsecretaría del Trabajo, Gobierno de Chile and Observatorio Laboral de la Región de Aysén, 2024). This region is particularly narrow, averaging about 50 km in width, and characterised by the presence of fjords which most of them are less than 5 km wide, numerous islands and intricate channels, restricting the water exchanges with the Pacific Ocean and shielding the Inner Sea (Sievers and Silva, 2008). This complex geography in addition to persistent cloud cover and heavy rainfall presents considerable challenges for observation and analysis (Díaz et al., 2025; Lara et al., 2017; Pantoja et al., 2011). Standard satellite products and global models, often limited by coarse spatial resolution, typically fail to resolve fjords and channels, and cannot capture the finer scale processes occurring in the most confined areas. Although high-resolution satellite products do resolve most of the fjords and channels, their temporal coverage and temporal resolution are not sufficient to calculate a long-term baseline, which should be based on at least 30 years of data according to WMO (2023) recommendations.

Despite its economic and environmental relevance, systematic temperature climatologies remain scarce in the region and are mostly based on satellite data (Narváez et al., 2019; Saldías et al., 2021; Vásquez et al., 2021), although regional and local climatologies have been derived from in situ datasets (Linford et al., 2023; Saldías et al., 2019). In complex regions such as Chilean Patagonia, in situ measurements are often the only reliable source for constructing consistent long-term climatologies. Over the last few decades, several oceanographic campaigns in the Northern Patagonian Seas have collected valuable physical and biogeochemical data across the region. However, these datasets are spatially and temporally irregular, making it challenging to generate consistent climatological fields. To date, no study has compiled these observations into a comprehensive, spatially resolved temperature climatology for Northern Patagonia.

To address this gap, this study employs the Data Interpolating Variational Analysis in n dimensions tool (DIVAnd, Barth et al., 2014; Troupin et al., 2012) to construct a temperature climatology for Northern Chilean Patagonia based on historical in situ records with a final resolution of about 900 m, effectively capturing all the fjords and narrow channels of Northern Patagonia. DIVAnd applies a variational interpolation approach that integrates data uncertainties, spatial correlation scales and topographic constraints making it particularly suitable for complex coastal environments. The objectives of this work are to describe the methodology used to generate the temperature climatology from historical observations, synthetise fragmented datasets into a coherent representation, evaluate its performance and discuss its potential for broader oceanographic applications in data-sparse regions.

2 Material and Method

2.1 Study area

Northern Chilean Patagonia is located in the south of Chile and represents the northernmost part of Chilean Patagonia (41–56° S). It spans from 41.4 to 46.7° S and from 72 to 74° W (Fig. 1). It is delimited to the east by the continent, to the north-west by the Island of Chiloé, and to the south-west by the Chonos Archipelago, composed of more than a thousand islands and playing a crucial role in reducing wind stress and mitigating waves intensity before they reach the mainland (Pinilla et al., 2019a). To the west of the sea, the continental shelf drops sharply, with depths increasing rapidly to over 2000 m due to the presence of the Peru-Chile Trench. The Northern Patagonian Fjords encompass diverse basins, channels and fjords. From north to south, the key areas include the large semi-enclosed gulf of Reloncaví Sound and the Reloncaví Fjord, which flows into the sound. To the south

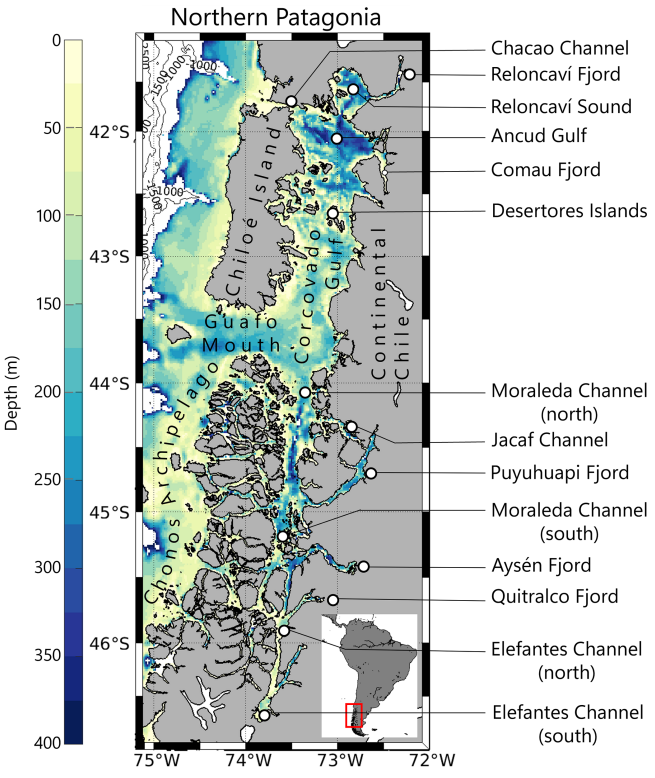


Figure 1. Map of the study area with bathymetry. Depth contours are shown at 500 m intervals while shallow bathymetry above 400 m is indicated by the colour shading.

of Reloncaví Sound lies the Ancud Gulf and the Corcovado Gulf, separated by the Desertores Islands, forming a natural barrier separating the deeper waters of Reloncaví Sound and Ancud Gulf from the shallower Corcovado Gulf. Ancud and Corcovado Gulfs are regions more influenced by oceanic waters entering through the Guafo Mouth (Calvete and Sobarzo, 2011; Pérez-Santos et al., 2014; Linford et al., 2023), with some fjords extending eastward into the continent. South of the Corcovado Gulf lies the narrow canal of Moraleda, which transitions into the Elefantes Channel, forming an extensive and complex network of channels and fjords (Soto-Riquelme et al., 2023; Linford et al., 2024). This particular geography makes it considered as a semi-enclosed sea, with the main connections to the ocean passing between Chiloé Island and Chonos Archipelago, a path called the Guafo Mouth (Sievers and Silva, 2008). The bathymetry in the Northern Patagonian Fjords is very complex due to its numerous microbasins and islands. Although the bathymetry is mainly shallower than 400 m, certain microbasins can be exceptionally deep, reaching for example 600 m in the Jacaf channel (Schneider et al., 2014; Pinilla et al., 2020).

2.2 Datasets

To construct the climatology, we gathered all available in situ temperature data to obtain a comprehensive dataset that best represents the region both spatially and temporally. The data come from various online repositories and direct field measurements, and were acquired using a range of sampling techniques, including CTD casts, drifting buoys and anchored moorings. Further details on data provenance are provided in Table 1 and in the supplementary material. Only observations located within the study area (75.1° W, 72.0° W and 41.4° S, 46.7° S) were retained, encompassing both surface and depth observations. All datasets were homogenised prior to merging, and variables were standardised to consistent units (°C for temperature and metres for depth). Data selection involved retaining only values flagged as valid when quality indicators were available, which means observations classified by the respective providers as "good", "valid" or "probably good", whereas observations flagged as "bad", "probably bad", "suspect" or otherwise invalid were excluded. Data considered "obviously wrong" (such as temperatures above 30 °C) were also excluded. In addition, for each major basin, the mean and standard deviation of temperature were calculated from the in situ observations, and any observation lying outside the range of mean $\pm$ 5 standard deviations were discarded. This relatively wide tolerance was chosen to preserve realistic extreme values while removing measurements that were physically implausible or likely to result from sensor errors (Garcia et al., 2024; Hoteit et al., 2009). Duplicate or near-duplicate observations were eliminated when the following criteria were simultaneously met: a horizontal distance of less than 0.01° (about 1 km), a vertical distance of less than 0.1 m, a sampling time difference of less than one day (given that many datasets have daily rather than hourly precision), and a temperature difference smaller than $\pm$ 0.1 °C.

In total, 3.3 million observations were used for the construction of the climatology, representing 5880 unique stations (Fig. 2A). The complete dataset spans the period from 1948 to September 2023, although spatial, vertical and temporal coverage are uneven (Fig. 2). Vertically, the measurements extend from surface to 400 m. Given that the climatology forms the core of our analysis, it was essential to use a reliable and representative dataset. The extensive spatial and temporal distribution of in situ measurements makes them well-suited for this purpose.

The inherently heterogeneous nature of in situ data results in variable sampling density through time and space. In particular, Comau Fjord was disproportionately sampled due to the long-term monitoring efforts of the Huinay Scientific Centre, which accounts for approximately 76 % of the total samples (Table 2). However, the other fjords and regions have also been relatively well sampled, though they represent a much smaller proportion of the total dataset (Table 2). Additionally, three anchored buoys were deployed

Table 1. Origin of the in situ data used for the construction of the climatology and information on the platform type, the institute that conducted the campaigns (if available), and the spatial and temporal extent of the samples. References are available in the Supplement.

Source/ Provider	Platform type	Institute	Temporal extent	Spatial extend	References
CMEMS	Drifting buoys	/	1 Jan 1950 to 31 Dec 2021	Entire study area	[1] to [6]
	CTD				
Pangaea	Shallow water monitoring stations	Wagner institute Huinay Scientific Field Station	7 Apr 2009 to 11 Feb 2014	Fjord Comau	[7] to [59]
				Fjord Renihue	
				Fjord Piti Palena	
				Repollal Islands	
World Ocean Database (WOD)	CTD (conductivity temperature depth)	/	23 Nov 1948 to 12 May 2020	Open Ocean, West of the Chiloé Island	[60]
	OSD (ocean station data)				
	XBT (expandable bathythermograph)				
	MBT (Mechanical Bathythermograph)				
	APB (Autonomous Pinniped Bathythermographs)				
	PFL (Profiling Floats)				
Centro de datos oceanográficos y meteorológicos (CDOM)	Anchored buoy	COPAS Sur-Austral	9 Mar 2013 to 19 Jun 2014	Reloncaví Fjord (Cochamo) 72.31° W, 41.52° S	http://cdom.cl/ (last access: 14 September 2022)
			1 Jul 2010 to 6 Apr 2018	Puyuhuapi Fjord 72.72° W, 44.58° S	
Centro de investigaciónes i∼mar	Anchored buoy	Centro de investigaciones i∼mar	28 Apr 2017 to 1 Sep 2023	Reloncaví Sound 72.8345° W, 41.6364° S	http://cdom.cl/
		COPAS Sur-Austral			
Centro de investigaciónes i∼mar	CTD	Centro de Instrucción y Capacitación Maritima (CIMAR)	20 Mar 1970 to 1 Sep 2022	Northern Patagonia	/
	Microprofiler (VMP-250)	Centro de investigaciones i∼mar			
		Instituto de Fomento Pesquero (IFOP)			

in Reloncaví Fjord, Reloncaví Sound and Puyuhuapi Fjord from 2010 onwards (Table 1), contributing significantly to the increased number of observations during the last decade in these basins. As a result, the temporal distribution of observations is strongly skewed towards recent decades: 99 % of the measurements were collected after 1990 and 55 % after 2010 (if considering only non-mooring data). The resulting climatology should therefore be interpreted as a climatological reconstruction based predominantly on recent observations (last three decades), rather than as an equally weighted 75-year climatological mean. Nevertheless, pre-1990 observations, though fewer in number, remain valuable as they include more than 1000 unique measurements that extend the time span of the climatological record back to 1948. Importantly, despite this temporal heterogeneity largely driven by a few intensively monitored sites, the overall spatial coverage remains extensive across the region (Fig. 3). Vertically, sampling is also heterogeneous, with approximately 70 % of all observations located within the upper 25 m of the water column (Fig. 2D).

To create a continuous field of the climatology of sea temperature in Northern Patagonia from sparse in situ data, we employed DIVAnd (Data-Interpolating Variational Analysis in n dimensions). DIVAnd is a spatio-temporal interpolation tool for geophysical variables that utilises scattered, spatially and temporally irregularly distributed data to create a continuous field.

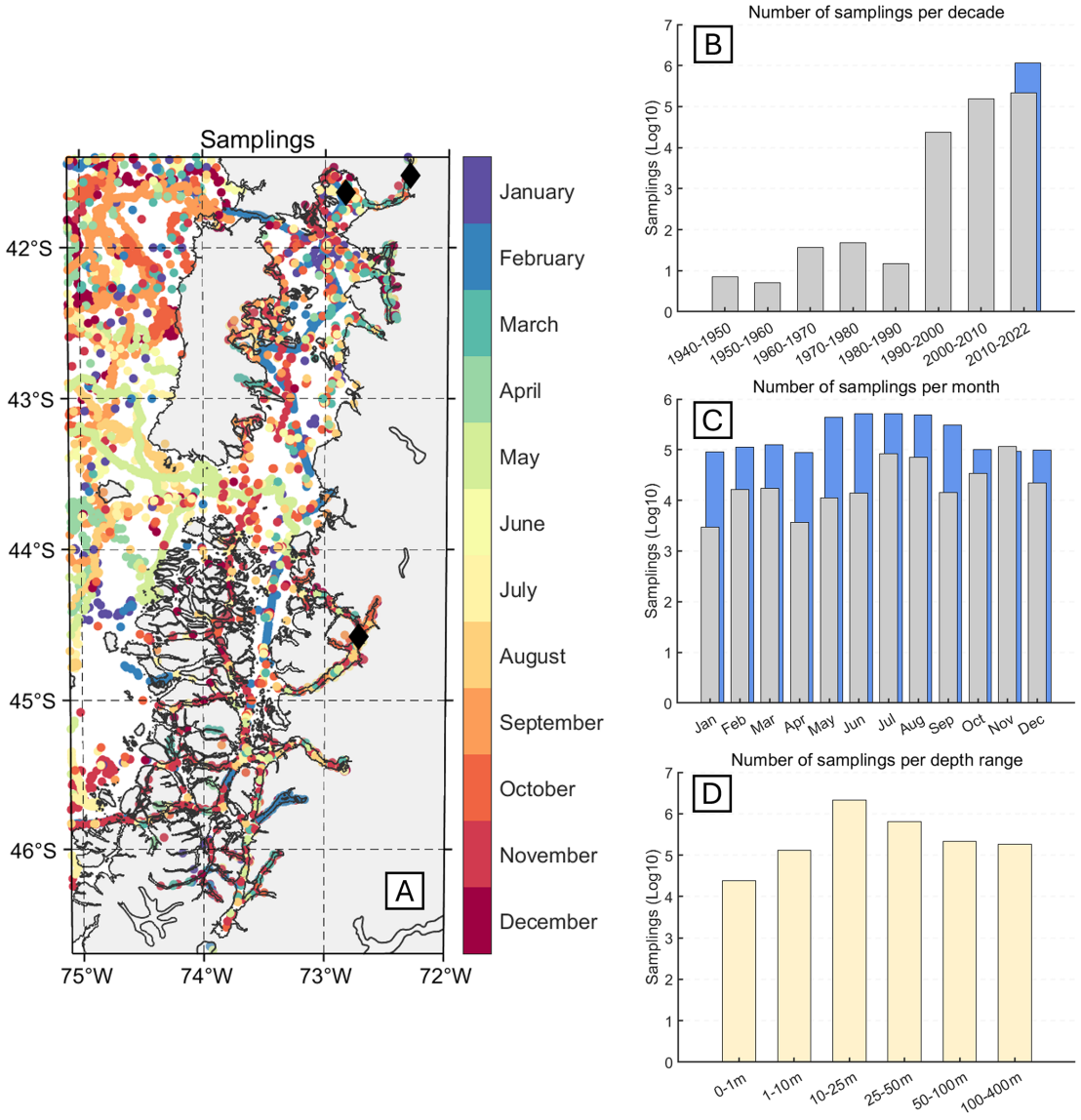


Figure 2. Spatial distribution of in situ observations (0–400 m depth), and the month during which they have been collected **(A)**. The three black diamonds in Reloncaví Sound, Reloncaví Fjord and Puyuhuapi Fjord represent the localisation of the three moorings. Temporal distribution **(B–C)** of the in situ observation over decades **(B)** and over months **(C)**. Vertical distribution **(D)** over certain depth ranges is shown. For **(B)** and **(C)**, grey bars represent the non-mooring data (i.e. from profiles and trajectory instruments), while blue bars represent the mooring data, and for **(D)** both mooring and non-mooring data are merged.

2.3 Construction of the temperature climatology

via variational interpolation, taking the bathymetry into account (Troupin et al., 2010; Barth et al., 2014). DIVAnd is an extension of DIVA (Data Interpolating Variational Analysis) for fields of more than 2 dimensions (Beckers et al., 2014; Brasseur and Haus, 1991; Troupin et al., 2012). This tool has been widely used for the construction of climatologies of many oceanic variables, from sparse data to continuous fields (Barth et al., 2021; Shahzadi et al., 2021a, b; Simoncelli et al., 2020). It is particularly well-suited for our study area since it can handle both spatial, temporal and vertical dimensions, allowing the interpolation of data in 2D (longitude × latitude), 3D (time or depth) or 4D (time and depth). The method is based on a variational inverse approach that minimises a cost function balancing two objectives: the analysed field should remain close to the available observations and it should exhibit a degree of spatial smoothness (Brasseur and Haus, 1991). Unlike a pure interpolation, DIVAnd does not force the resulting field to pass exactly through each observation, as measurements can be subject to errors and may not fully represent the environmental conditions (Janjić et al.,

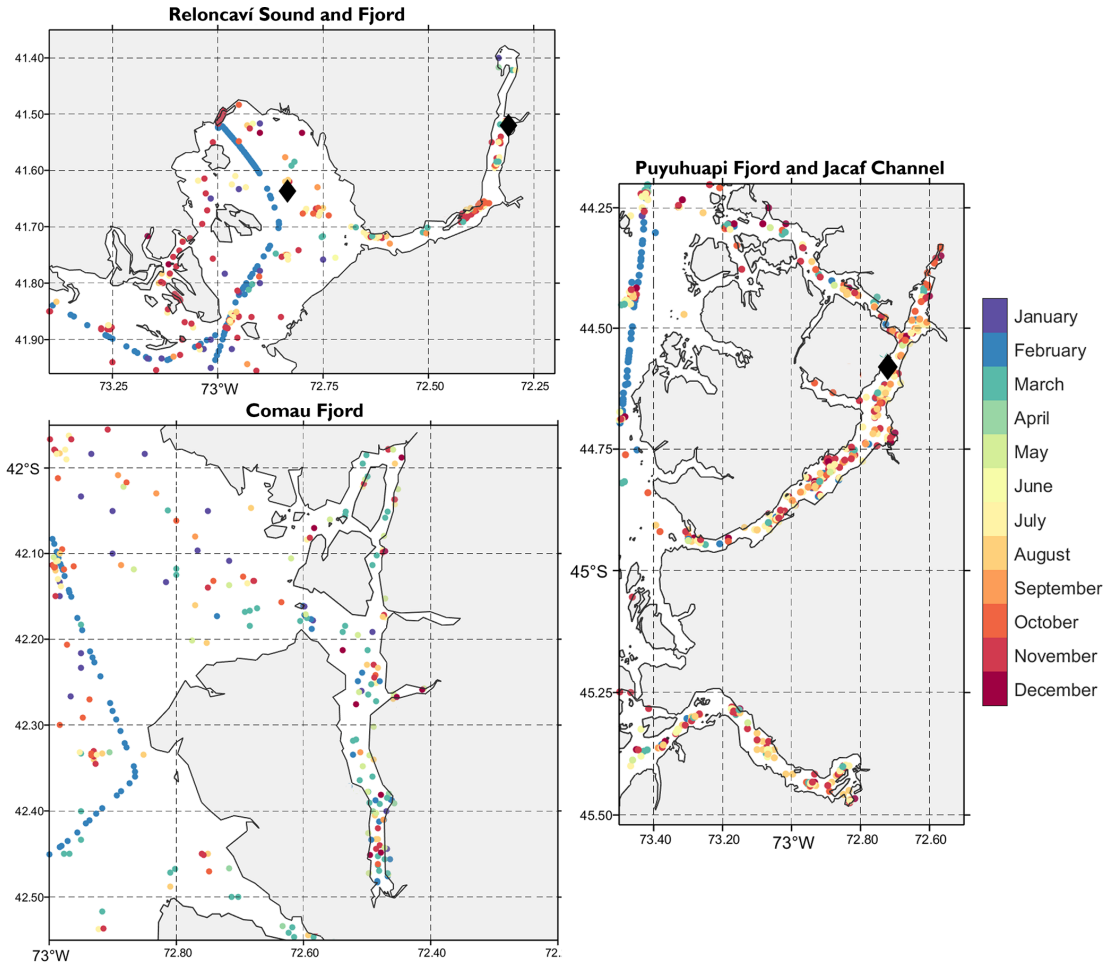


Figure 3. Spatial distribution of in situ observations (0–400 m depth), and the month during which it has been collected in specific regions. Black diamonds indicate the location of anchored buoys.

2018). The cost function is detailed below in Eq. (1):

$$J(\varphi) = \sum_{j=1}^{\mathrm{Nd}} \mu_j \left[d_j - \varphi\left(x_j\right)\right]^2 + \|\varphi - \varphi_\mathrm{b}\|^2 \quad (1)$$

where φ is a scalar ocean field defined in our case as the temperature, and d_j are the Nd measurements of the field φ at the location x_j for a given time, with their associated weight μ_j. φ_b is a background estimate of the field, representing a first guess of the field to be interpolated. The norm $\|.\|^2$ also involves spatial/temporal derivatives of the field to penalise abrupt variations. The computation was performed using DIVAnd v2.7.12 available as a package in the Julia programming language and in conjunction with Jupyter Notebooks (https://github.com/gher-uliege/DIVAnd.jl, last access: 25 July 2022). The variable to be interpolate in this study was the temperature, with the objective of building a 4D climatology. The required input consists of a dataset of potentially irregularly distributed observations, with associated coordinates (longitude and latitude), depth and date.

To generate a fine-scale spatio-temporal climatology from in situ surface and subsurface data, we first computed a background field, which is a first guess representation of the temperature distribution that served as the basis for the subsequent monthly climatology (Barth et al., 2021). This background field was produced at a seasonal temporal resolution by grouping months into four standard seasons: January–February–March (austral summer), April–May–June (autumn), July–August–September (winter), October–November–December (spring). For each season, only the in situ observations corresponding to the relevant months were used. This approach mitigates the uneven temporal coverage and spatial gaps in the dataset, particularly in regions and periods with limited sampling, and provides a representative mean seasonal state of the temperature field. The result is an averaged representation of the study area over the time period 1948–2023 with seasonal temporal resolution.

The monthly climatology was then derived by refining the background fields. For each month, the corresponding sea-

Table 2. Spatial repartition of samplings (at all depths) in different regions of the study area. The second column indicates the total number of samplings in an area, while the third one shows which proportion those samplings represent among the entire study domain.

Region	Samplings	Proportion of samplings (%)
Reloncaví Sound	76 206	2.26
Reloncaví Fjord	35 158	1.04
Ancud Gulf	53 604	1.59
Comau Fjord	2 587 816	76.83
West of Chiloé Island	25 221	0.75
Corcovado Gulf	299 623	8.89
Guafo Mouth	10 937	0.32
Moraleda Channel	52 668	1.56
Chonos Archipelago	31 879	0.95
Puyuhuapi Fjord	110 604	3.28
Elefantes Channel	10 637	0.32
West of Chonos Archipelago	5615	0.22

sonal grid was used as the background field, and all available in situ observations from that month were incorporated to enhance spatial and temporal detail. This two-step approach ensured that the monthly climatology remained dynamically and statistically consistent with broader seasonal patterns while resolving finer-scale monthly variability. The outcome is a set of twelve fields, corresponding to a monthly climatology (monthly temporal resolution), each representing the mean temperature state for every grid cell of the study area for the period 1948–2023. Both the seasonal background and the monthly climatology share identical vertical and horizontal resolutions and were processed following the same methodological framework.

For both products (background and climatology), the configuration of DIVAnd was designed to balance data fidelity and spatial smoothness, ensuring a robust and physically consistent representation of the temperature field. To reduce the influence of spatially clustered measurements, the DIVAnd weighting function was applied with a 0.1° (∼ 10 km) threshold for cluster identification. The interpolation smoothness was tuned using correlation length scales of 50 km horizontally and 50 m vertically, which define the spatial influence of the observations. The noise-to-signal ratio, representing the error variance relative to the background error variance, was set to 0.01 and scaled by the previously assigned weights. Parameter values were selected to optimise performance metrics obtained from independent validation tests. The final gridded fields were produced with a 0.008° (approximately 900 m) horizontal resolution, reaching our computational limits, representing a horizontal grid of size 357×751, covering the Northern Chilean Patagonian fjords between 75.1 to 72° W and 47 to 41° S. Bathymetric constraints were derived from GEBCO dataset which has a spatial resolution of 30 arcsec (https://www.gebco.net/data_and_products/gridded_bathymetry_data/, last access: 6 December 2021). As approximately 70 % of the observations were collected within the upper 25 m, climatologies were computed on a non-uniform vertical grid to reduce near-surface bias. Temperature was interpolated onto 32 unevenly spaced depth levels ranging from the surface to 400 m, with finer spacing near the surface (0, 2.5, 5, 7.5, 10, 12.5, 15, 17.5, 20, 25, 30, 35, 40, 45, 50, 60, 70, 80, 90, 100, 125, 150, 175, 200, 225, 250, 275, 300, 325, 350, 375, 400 m). The DIVAnd interpolation resulted in a monthly climatology at 32 different depths with a resolution of approximately 900 m, effectively resolving all fjords and channels from the northern Patagonia.

2.4 Validation and performance of the climatology

To assess the performance of the monthly climatology and validate it, 5 % of the in situ observations were put aside from the reconstruction process and used for independent validation (see Table 3 and Tables S1–S3 for details). This procedure was performed separately for four validation depths: the surface, 30, 100 and 200 m. The validation was carried out over depth intervals centred on each target depth rather than at the exact depth itself, in order to retain a sufficient number of independent observations: 0–1 m for the surface, 25–35 m for 30 m, 90–110 m for 100 m, and 180–220 m for 200 m. These intervals are narrower near the surface, where temperature varies more strongly with depth, and wider at depth, where the vertical temperature gradient is weaker and observations are sparser. At each depth interval, the withheld observations were used to evaluate the reconstructed temperatures independently of the data used for interpolation. The subsets were selected randomly across space and time to ensure representative coverage of the study area. However, for the anchored moorings, random temporal sequences of varying lengths were withheld instead of isolated points, in order to provide a more robust validation of the reconstructed temporal variability. Validation was performed separately for each monthly field by comparing the reconstructed and observed temperatures. Statistical performance was quantified using the correlation, the bias, the root mean square error (RMSE), the centred root mean square error (CRMSE), and the standard deviation. Together these metrics evaluate both the strength of the relationship and the magnitude of residual errors between independent observations and the reconstructed field (climatology). Validation was not extended below 200 m because the number of available in situ observations decreases substantially with depth. Withholding 5 % of the observations at these depths would have further reduced the already sparse data available for reconstruction, potentially compromising the interpolation. Moreover, the limited number of independent observations would have made the resulting validation statistics less representative and dependable.

To further assess the spatial consistency of the reconstruction and account for the uneven distribution of observations across the study area, regional validation was performed for the surface layer. The same statistical metrics as described above were calculated separately for five main regions: Reloncaví Sound, Ancud-Corcovado Gulfs, Comau Fjord, Chonos Archipelago-Moraleda region, and the Puyuhuapi-Aysén Fjords.

DIVAnd also provides a relative analysis error field associated with the interpolated temperature, which quantifies the remaining uncertainty of the analysis relative to the background error variance allowing the user to assess the spatial and vertical confidence of the climatology (Beckers et al., 2014). This error field is adjusted according to the weighting function and the noise-to-signal ratio chosen prior to the interpolation in DIVAnd. The relative error ranges from 0 to 1, with lower values indicating that the analysis is more strongly constrained by the observations resulting in high confidence, while higher values indicate greater remaining uncertainty, meaning that the analysis relies more heavily on the background field (i.e. first guess) and is less constrained by the observations. The relative analysis error is influenced by the spatial and temporal distribution of the observations, their associated uncertainties, the specific correlation length scales, and the geometry of the interpolation domain, including physical boundaries. It therefore provides an additional measure of the spatial and vertical observational constraint of the reconstructed climatology.

Many oceanographic and ecological applications require daily climatologies to capture short-term physical or biological variability more accurately (e.g. Hemming et al., 2020; Hobday et al., 2016). We therefore derived a daily climatology from the monthly fields described in the previous section. Because the number of observations decreases with depth, the daily-derived climatology was limited to the upper 100 m on the same 14 vertical levels as the monthly climatology (i.e. 0, 5, 10, 15, 20, 25, 30, 40, 50, 60, 70, 80, 90 and 100 m). This choice avoids extending the temporal interpolation to deeper layers where observational support is more limited. To convert the monthly climatology into a daily time-scale product, each monthly field was expanded over the corresponding number of days in that month (for instance, the January field was repeated 31 times, February 29 times, March 31 times, etc.) This produced a continuous sequence of 366 daily fields with the same spatial characteristics as the monthly fields. To smooth the resulting daily time series and ensure a physically realistic and gradual transition between months, a 90 d centred moving average was then applied to each grid cell. This temporal filter mitigates abrupt discontinuities at month boundaries and yields a continuous, smoothed representation of the annual temperature cycle. The choice of a 90 d window balances temporal smoothness and the preservation of the seasonal signal, consistent with similar approaches in constructing high-frequency climatologies.

The resulting dataset (later referred to as the "daily-derived climatology" in the manuscript) provides one representative value per day of the year for each grid cell, ensuring internal consistency with the monthly product while allowing finer temporal analyses and comparison with daily observational or model data. This approach preserves the large-scale seasonal and monthly variability of the original climatology, without attempting to reproduce intra-monthly variability that is not resolved by the available in situ data in most of the basins.

Both climatology fields are distributed as NetCDF3-Classic files using geographical coordinates referenced to the WGS84 coordinate reference system. The files are available online through the repository indicated in the Data Availability section.

3 Results

3.1 Validation of the climatology

To validate the monthly climatology, 5 % of the in situ data was set aside and excluded from the reconstruction process at four targeted depths (see Methods). These independent subsets were then used to evaluate the accuracy of the monthly climatology through statistical comparisons. Overall, the results indicate that the monthly climatology reproduces the spatial and seasonal variability of surface temperature with reasonable accuracy (Tables 4 and S4–S6 in the Supplement).

In the surface layer, biases between the interpolated field and the observations are small throughout the year (ranging from −0.139 to +0.214 °C) and RMSE values rarely exceed 1 °C, suggesting a robust representation of the mean state. Correlation coefficients exceed 0.7 from June to September, when surface waters are the coldest and show less variation, while lower correlations and higher errors are found in summer months, reflecting stronger small-scale variability and stratification. January and April display the lowest correlations (0.159 and 0.171, respectively), consistent with the limited number of available in situ observations (99 and 161 respectively, compared to an average of 485 per month). The CRMSE is close to the RMSE for all months, indicating that most of the errors arise from spatial variability rather than from a systematic bias. The standard deviation of the climatology is consistently smaller than that of the in situ data, meaning that the reconstructed fields are smoother than the original observations, which is an expected feature for a climatological product.

When comparing the interpolation errors with the natural variability of the system, RMSE values are generally smaller than the standard deviation of the in situ data during the austral summer, indicating that the climatology successfully captures the large-scale temperature patterns. In contrast, during winter months, RMSE slightly exceeds the standard deviation of the observations, showing that even small absolute errors can represent a significant fraction of the re-

Table 3. Total number of observations collected at the sea surface (0–1 m depth), separated into mooring and non-mooring sources (mooring observations and non-mooring observations), along with the 5 % of each group set aside for validation (mooring validation and non-mooring validation).

Month	Total observations	Mooring observations	Mooring validation	Non-mooring observations	Non-mooring validation
Jan	8792	8693	435	99	5
Feb	14 680	13 685	684	995	50
Mar	13 921	13 711	686	210	11
Apr	8534	8373	419	161	8
May	10 081	9478	474	603	30
Jun	9409	9077	454	332	17
Jul	9825	9331	467	494	25
Aug	9022	8557	428	465	23
Sep	10 289	9540	477	749	37
Oct	9659	9174	459	485	24
Nov	8712	7701	385	1011	51
Dec	9238	9020	451	218	11

duced thermal variability typical of this period. Since RMSE quantifies the difference between the monthly climatology and instantaneous in situ measurements, it also encompasses sub-seasonal and interannual variability. Consequently, even a perfect climatology derived from an unlimited number of observations would not achieve a zero RMSE or a correlation of one.

To assess whether the domain-wide validation results were representative of the different hydrographic environments and not disproportionately influenced by the uneven spatial distribution of observations, the same metrics were additionally calculated separately for the main regional basins. The regional validation further indicates that the reconstruction performance is broadly consistent across basins. RMSE values are higher in the Ancud-Corcovado and Puyuhuapi-Aysén regions in January (1.81 and 2 °C respectively) and February, but remain below 1 °C during the other months, following a pattern similar to the domain-wide statistics. The larger errors in the Puyuhuapi-Aysén region are consistent with the higher temperature variability of that region (standard deviation exceeding 2 °C in summer). The Reloncaví region shows a comparable seasonal pattern, with RMSE values below 1 °C from April to November and peak errors in January. In the Chonos-Moraleda region, RMSE values remain below 1 °C throughout the year, although these relatively low errors should be considered in relation to the comparatively low standard deviation of the observations in this region. Finally, Comau Fjord, accounting for the largest proportion of observations, shows relatively low RMSE values throughout the year (< 1 °C). Overall, the reconstruction errors remain consistent with the magnitude of natural temperature variability across the different regional environments, confirming that the good performance observed for the entire domain is also broadly maintained at the regional scale.

The subsurface validation also indicates good reconstruction performance (Table S4). At 30 m depth, correlation coefficients are generally higher than at the surface, ranging from 0.628 in February to 0.955 in September. This February minimum coincides with the largest positive bias (+0.254 °C) and the largest RMSE (0.441 °C). Biases remain small throughout the year (from −0.1 °C in June to +0.254 in February), and RMSE and CRMSE values remain below 0.5 °C. Contrary to surface, RMSE and CRMSE show on certain months a larger difference between RMSE and CRMSE. The standard deviation of the reconstructed climatology can be higher than the standard deviation of the in situ data used for the reconstruction, which contrasts with the surface behaviour, where the climatology was systematically smoother than the observations. It suggests that the reconstruction can show higher variability than the in situ observations. However, the RMSE values remain smaller than the standard deviations, indicating that the climatology captures a substantial fraction of the subsurface signal.

At 100 m depth, the validation statistics indicate that the reconstruction remains accurate, although with a different signature than at the surface (Table S5). Correlation is consistently high throughout the year, ranging from 0.855 in October to 0.996 in January, with a single notable exception in April, when the correlation drops to 0.537. It is important to note that both January and April coincide with few available in situ observations at this depth (respectively 155 and 197 observations, see Table S2). Biases are small and predominantly negative (from −0.055 °C in January to +0.016 °C in April), indicating a slight cold bias of the climatology relative to the observations.

As for the upper layers, CRMSE and RMSE show near-identical values, both remaining below 0.3 °C in all months and reaching a minimum RMSE in September. The standard deviation of the reconstructed climatology is always lower

than that of the in situ observations, except in January, indicating that the subsurface fields are also smoother than the original observations, consistent with the expected behaviour of a climatology. The RMSE is also always lower than the standard deviation of the in situ data, showing that the climatology captures a large fraction of the subsurface temperature signal.

At 200 m depth, the validation results indicate generally good agreement between the reconstructed climatology and the independent observations, although data availability limits the calculation of validation statistics for some months. No reliable statistics could be obtained for January and April because, despite the availability of in situ observations at these depths, few of them coincided with locations where the climatology provided interpolated values. For the remaining months, correlation coefficients exceed 0.86, reaching 1 in May (however this result should be interpreted with caution because only five observations were available for validation). Biases remain small, ranging from −0.093 to 0.123 °C, and RMSE values remain below 0.35 °C. The standard deviation of the reconstructed fields is generally lower than, or comparable to, that of the in situ observations, suggesting that the reconstructed fields are smoother than the observed temperature variability. RMSE values are consistently lower than the standard deviation of the in situ observations, indicating that the reconstruction errors are smaller than the observed temperature variability.

Overall, the validation at the four targeted depths confirms that the generated climatology is consistent with the available observations. The errors remain of the same order as, or smaller than, the natural variability of the system, and the RMSE-CRMSE comparison indicates that spatial variability, rather than systematic bias, dominates the error budget at the surface, 100 and 200 m, whereas a small systematic component is present at 30 m in some months. The largest errors found at 30 m depth might be explained by the vertical influence of the highly variable upper layers. Lower performances are also observed during months of limited independent observations.

Altogether, the climatology provides a reliable baseline for representing surface temperature variability in Northern Chilean Patagonia from the surface to 200 m depth (greater depths were not analysed due to lack of independent observations). The complete climatology (both monthly and daily-derived) is freely available at https://doi.org/10.5281/zenodo.21959707 (Pujol et al., 2026) with two companion codes (MATLAB and Jupyter Notebook Python 3) for easy data handling and visualisation.

3.2 Description of the climatology

3.2.1 Surface temperature patterns

Before examining the monthly fields, the seasonal background climatology provides an overview of the large-scale thermal structure of Northern Chilean Patagonia (Fig. 4). These background fields, computed as the first step of the DIVAnd interpolation over all 32 depth levels (0–400 m) following the same vertical structure as the monthly climatology, summarise the dominant spatial patterns for summer, autumn, winter and spring. At the surface, they clearly highlight a strong temperature gradient during summer in the Pacific Ocean, and warm regions in the inner sea, such as Reloncaví Sound and Fjord, and Puyuhuapi Fjord. Autumn shows a progressive cooling of the region, with a north-south gradient, relatively uniform temperatures in winter, and warming in spring. The seasonal backgrounds reveal the persistent west-east gradient in summer, and the marked cooling of the southern fjords in winter, particularly Aysén Fjord. These backgrounds were used for the subsequent monthly DIVAnd analyses, ensuring that the interpolation respects the main seasonal structure while allowing finer monthly features to emerge.

The DIVAnd-interpolated monthly climatology captures the mean thermal structure and seasonal variability of Northern Chilean Patagonia, based on in situ observations. The product spans 32 depth levels, from the surface to 400 m, and reveals consistent spatial and vertical temperature patterns across the region (Figs. 5–8 and S1–S32 in the Supplement).

At the surface (Fig. 5), the climatology reveals marked seasonal and spatial variations. During summer (January–February–March), strong west-east temperature gradients are observed in both the open Pacific and Northern Patagonia, particularly in Reloncaví Sound and Ancud Gulf. Most of the study area records temperatures between 12 and 14 °C, with local maxima in February reaching approximately 18 °C in Puyuhuapi Fjord, 17 °C in Reloncaví Sound and Fjord and in the north-western open ocean, and 16 °C in Comau Fjord. Despite being located only 50 km south of Puyuhuapi Fjord, Aysén Fjord reaches only 13 °C in February, highlighting its cooler conditions. The Chacao Channel and the area south of the Desertores Islands stand out as particularly cold regions throughout the summer.

During autumn (April–May–June), surface temperatures gradually decrease, though a weaker west-east gradient persists. By June, a clear north-south gradient becomes apparent in Northern Patagonia with values ranging from 10–11 °C in Reloncaví Sound to about 8 °C in the southernmost part of the domain.

Winter (July–August–September) is characterised by uniform surface temperatures and minimal spatial variability. Most areas remain around 10 °C, with the lowest values of about 8 °C in Puyuhuapi Fjord and 7 °C found in the Elefantes Channel and Aysén Fjord. A slightly warmer patch southwest of Chiloé Island in July can be observed, but it likely results from an anomalous measurement or uneven temporal sampling.

In spring (October–November–December), gradual warming resumes with the development of the west-east gradient

Table 4. Statistic metrics for the validation of the monthly climatology at the surface level only (independent observations between 0 and 1 m) for every month: Correlation, Bias (°C), Root mean square error (RMSE, °C), Centred root mean square error (CRMSE, °C), the average Standard deviation (SD, °C) across the entire study area for the climatology, the average Standard deviation for the in situ data used for the climatology construction between 0 and 1 m depth, and the average Standard deviation (°C) across the entire study area for the entire in situ dataset.

Month	Correlation	Bias	RMSE (°C)	CRMSE (°C)	SD climatology	SD in situ	SD in situ full dataset
Jan	0.159	0.214	1.847	1.834	1.160	2.025	1.974
Feb	0.709	0.039	1.433	1.433	1.274	2.359	2.054
Mar	0.320	0.112	1.141	1.135	1.019	1.362	1.685
Apr	0.171	−0.068	1.006	1.004	0.910	1.198	0.830
May	0.558	−0.082	0.783	0.779	0.937	1.013	0.774
Jun	0.810	−0.083	0.709	0.705	1.002	1.329	0.458
Jul	0.806	0.062	0.872	0.870	0.811	1.535	0.594
Aug	0.821	−0.139	0.707	0.693	0.536	1.255	0.580
Sep	0.748	0.010	0.731	0.731	0.608	1.204	0.511
Oct	0.396	0.202	0.952	0.930	0.672	1.216	0.817
Nov	0.410	0.086	1.232	1.229	0.738	1.580	1.234
Dec	0.446	0.105	1.421	1.417	1.081	1.800	2.184

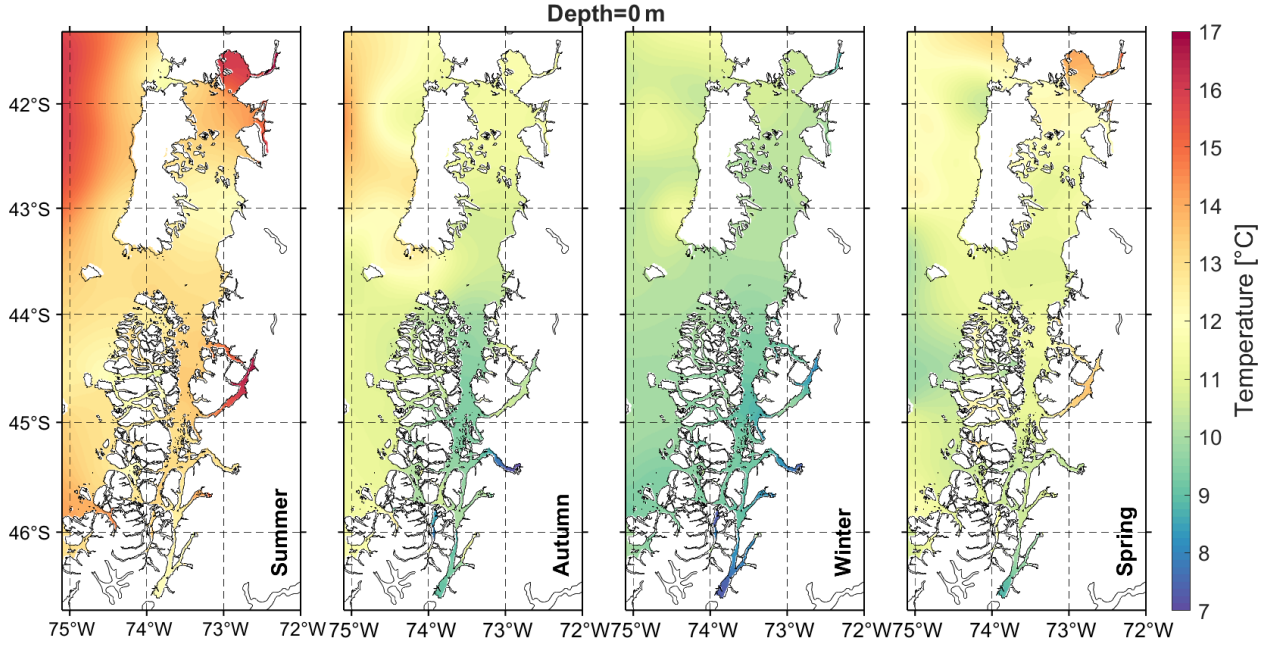


Figure 4. Background seasonal fields of the interpolation for surface.

and pre-summer conditions established by December. Temperatures reach 15 to 17 °C in Puyuhuapi Fjord and Reloncaví Sound, while colder waters (below 11 °C, locally down to 9 °C) persist in southern Northern Patagonia and west of the Chonos Archipelago.

These spatial patterns are associated with marked seasonal contrasts, with temperature amplitudes varying significantly between open and enclosed basins. Indeed, temperature fluctuations are stronger in enclosed fjords and sounds. Reloncaví Sound varies between 10 °C in winter and 17 °C in summer. Puyuhuapi Fjord ranges from 8 °C at its head in winter to 18 °C in summer (9–16 °C in its central part), and Aysén Fjord exhibits a seasonal range of 6 to 13 °C at its head and 9 to 13 °C near its mouth. In contrast, open basins show smaller seasonal amplitudes: Corcovado Gulf (10–13 °C), Moraleda Channel (9–13 °C) and Ancud Gulf (11–14 °C). The open Pacific west of Chiloé Island experiences a wider range (10–17 °C), whereas west of the Chonos Archipelago, seasonal variability is more moderate (9–13 °C).

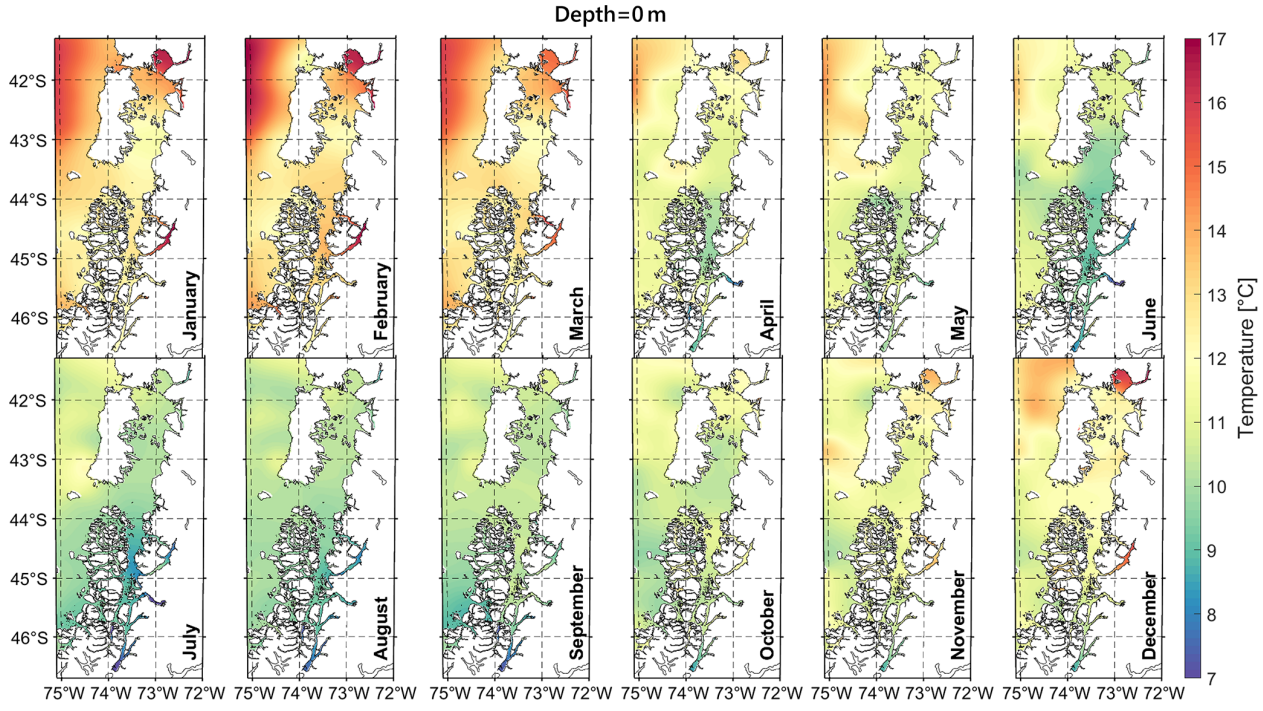


Figure 5. Monthly climatology of the sea temperature at the surface.

3.2.2 Subsurface structure

Below the surface, temperatures decrease with depth and horizontal gradients weaken, especially during summer. At 30 m depth, the field becomes nearly homogeneous in winter, whereas in summer it varies from 14 °C west of Chiloé Island to 10 °C in the south (Fig. 6). At 100 m depth (Fig. 7), temperatures remain relatively stable throughout the year around 10 °C, with slightly warmer conditions (about 11 °C in winter and 12 °C in summer) in Ancud Gulf and Reloncaví Sound and their associated fjords. At 200 m depth, these northern basins remain slightly warmer (10–11 °C) than the rest of the region (8–9 °C). At 400 m, temperatures stabilise near 7 °C across the entire domain year-round, except in Aysén Fjord, where values oscillate between 10 °C (July–December) and 8.5 °C (January–June). This seasonal pattern aligns with in situ measurements collected over multiple years, suggesting relatively slow temperature adjustment in this fjord.

The vertical temperature distribution highlights a strong seasonal variation of stratification in Northern Patagonia (Fig. 8). Four regions are described, and the comparison between the original observational vertical profiles and the climatology results are available in Fig. 8. In most basins, the thermocline typically lies between the surface and 20 m depth and strengthens during summer, as illustrated for Reloncaví Sound (Fig. 8A, B). It can deepen to 50 m west of Chiloé Island or within Aysén and Puyuhuapi Fjords (Fig. 8G, H), and even extend down to 100 m in the Guafo Mouth and Corcovado Gulf (Fig. 8E, F). In winter, the entire water column is nearly homogeneous, especially around the Chacao Channel, the northern half of Corcovado Gulf and Ancud Gulf (Fig. 8C, D). The surface mixed layer is generally shallow in summer (less than 10 m) with pronounced surface stratification in fjords and semi-enclosed basins.

The proportion of the study domain covered by interpolated values decreases progressively with depth, reflecting the bathymetry characteristics of the fjord environment. The interpolation covers 100 % of the domain at the surface and remains relatively high in the upper 100 m, with more than 65 % of the domain containing valid interpolated values. Coverage then decreases substantially with depth, reaching approximately 30 % at 200 m and only 14 % at 400 m. At 400 m, the interpolated area is primarily confined to the Peru-Chile Trench west of Chiloé Island and a few deeper-micro-basins within the fjord system.

4 Climatology performance

Unlike the surface validation, a comparable quantitative assessment using withheld observations is not feasible for the full four-dimensional climatology, as withholding the already sparse subsurface data could degrade the reconstruction. Instead, we evaluate the observational constraint of the interpolated fields using the relative analysis error provided by DIVAnd. The DIVAnd relative error fields reveal substantial spatial, temporal and vertical variability in the observational constraint of the reconstructed temperature fields, with variations that closely follow the distribution of obser-

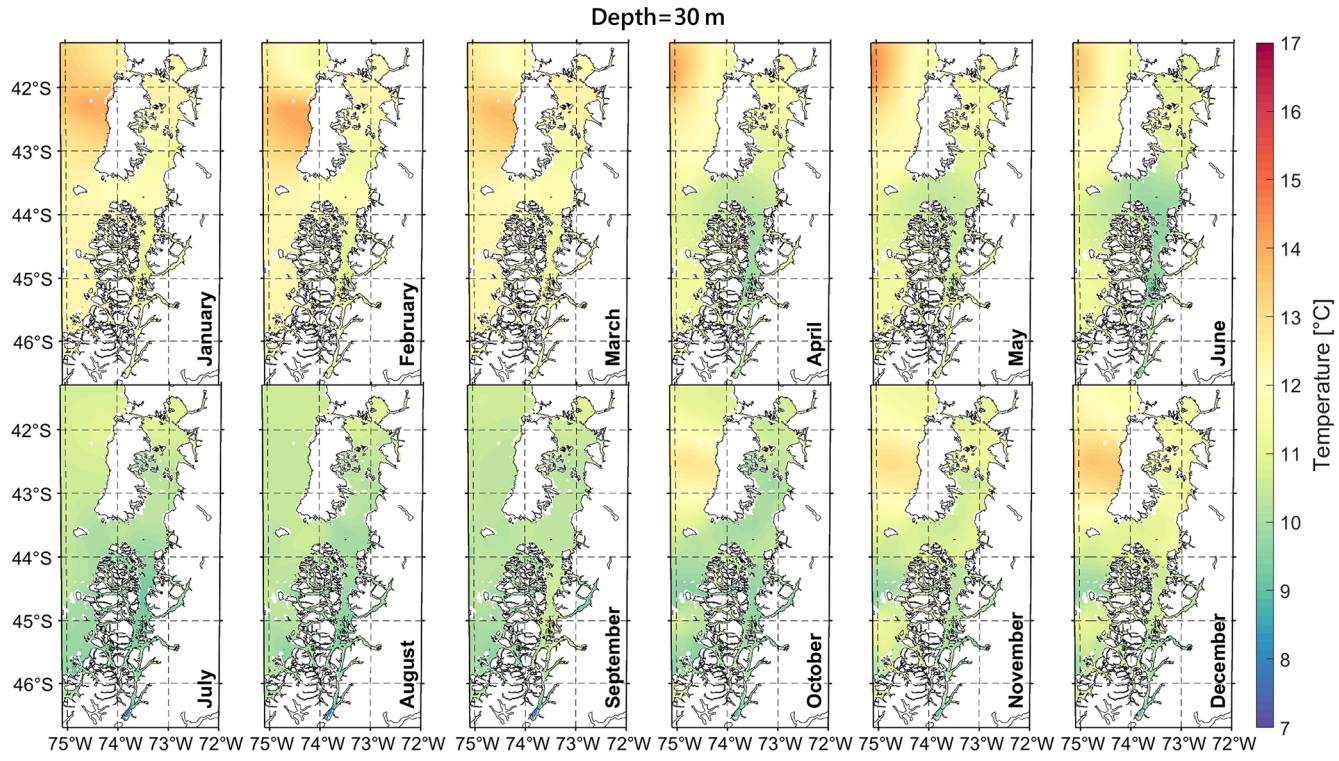


Figure 6. Monthly climatology of the sea temperature at 30 m depth.

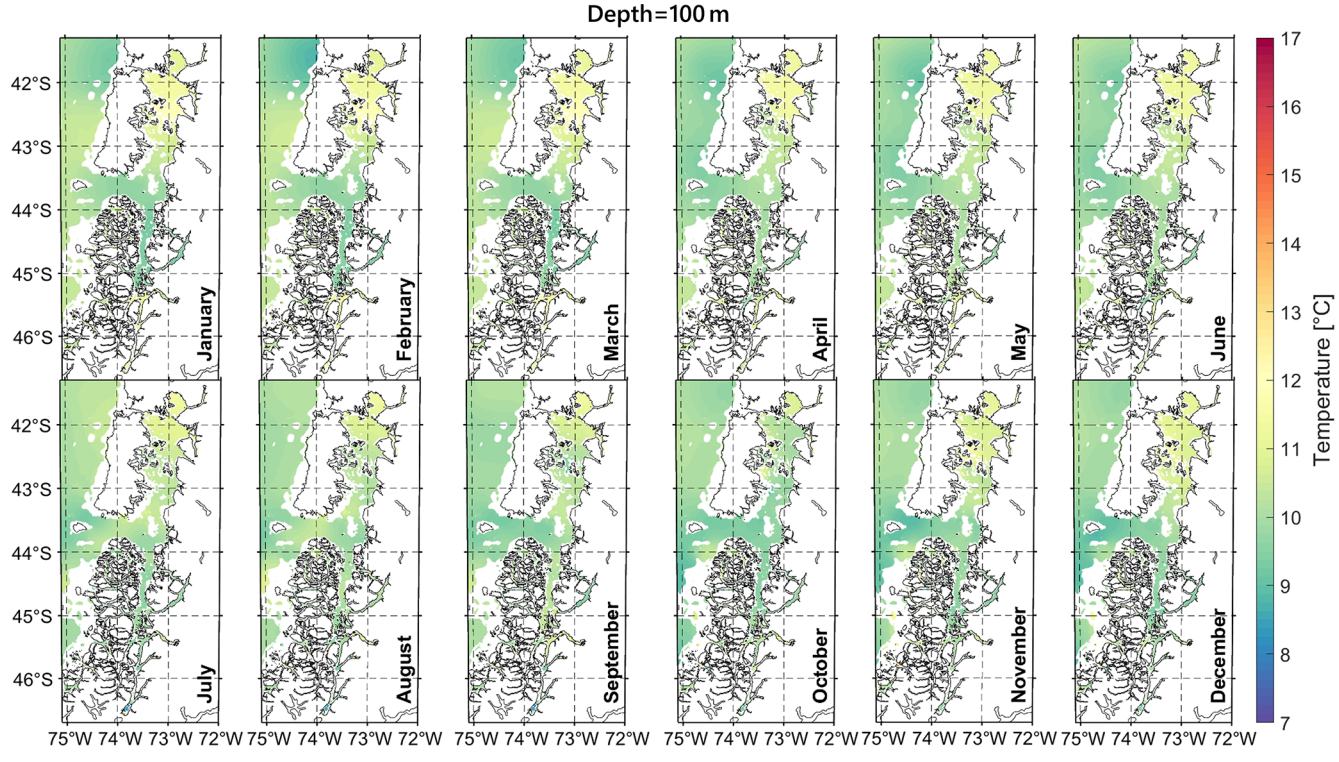


Figure 7. Monthly climatology of the sea temperature at 100 m depth.

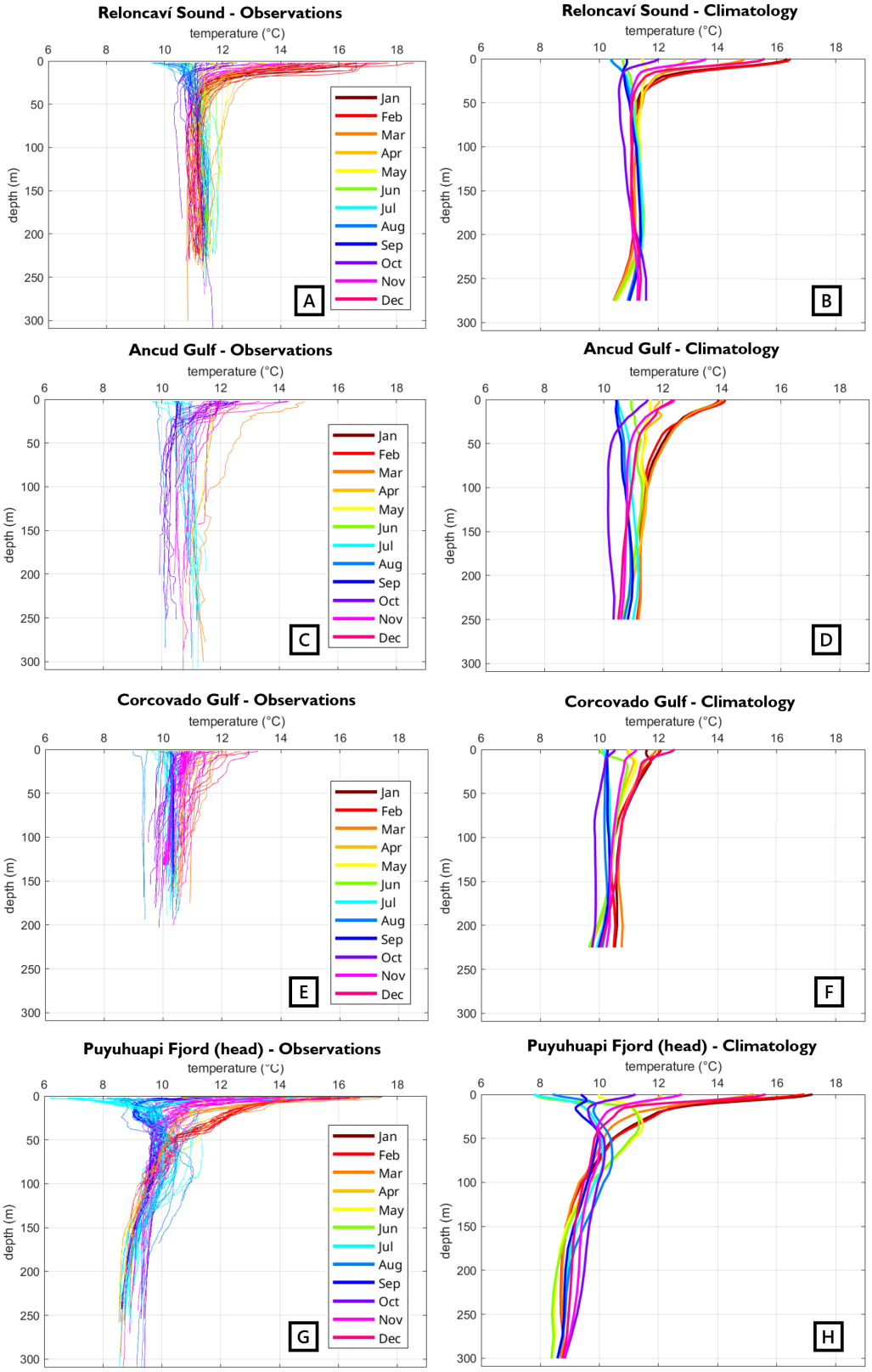


Figure 8. Profile plots of the in situ observations (left) and the monthly climatology in different basins of the study area: **(A–B)** Reloncaví Sound, **(C–D)** Ancud Gulf, **(E–F)** South of the Corcovado Gulf, **(G–H)** the head of Puyuhuapi Fjord. Each colour represents the monthly climatology for a specific month of the year. The profile terminates according to the local bathymetry.

vations (Figs. 9–11 and S33–S64). At the surface, relative errors are generally low throughout the study area, particularly within the fjords and channels, indicating that these areas are strongly constrained by the available observations (Fig. 9). Conversely, higher relative errors are observed where the observations are comparatively sparse. January and April, which are the two least-sampled months of the dataset, represented by respectively only 99 and 161 non-mooring surface observations (Table 3), exhibit some of the highest relative errors in Northern Patagonia, particularly in the southern part of the domain, resulting in a comparatively weak observational constraint. In contrast, months with more extensive observational coverage generally exhibit lower relative errors, particularly within Northern Patagonia.

A pronounced vertical structure is also evident in the relative error fields. The relative error generally increases rapidly with depth, particularly evident west of Chiloé Island, where the available observations consist predominantly of surface drifters and therefore provide limited constraint below the surface. The strongest relative error variations occur within the first 30 m, reflecting the rapid decrease of available observations for the interpolation (Fig. 10). From January to June, the relative error fields show greater spatial variability, reflecting the uneven availability of observations during these months compared with the second half of the year. January generally exhibits the weakest observational constraint, while relative errors remain very low (below 0.1) in all of Northern Patagonia from July to December. Throughout the year, relative errors are generally close to zero in the different fjords.

Below 30 m depth, the spatial structure of the relative error remains broadly similar down to approximately 100 m, although some regions show a progressive reduction in observational constraint with depth (Fig. 11). Some basins remain characterised by low relative errors (generally below 0.3) over the entire water column, indicating that the interpolation remains relatively well constrained even at depth. This is particularly noteworthy given the substantially lower availability of observations at depth compared with the surface. The four regions of Reloncaví Sound Reloncaví Fjord, Comau Fjord and Puyuhuapi Fjord show relative errors close to zero as they are regions covered by moorings and very high sampling densities. Reloncaví Sound is the only region showing relative errors below 0.3 throughout the year, due to the fact that it is a particularly well sampled region, including subsurface measurements. In contrast, relative errors approaching 1 are predominant in the Pacific Ocean, where subsurface observations are nearly absent and the analysis therefore retains a large fraction of the background uncertainty.

5 Discussion

In this study, a 4-dimensional climatology was constructed from in situ observations spanning 75 years in Northern Chilean Patagonia, a region characterised by highly complex bathymetry, strong freshwater inputs, and an intricate network of fjords and channels (Pantoja et al., 2011; Rodrigo, 2008; Strub et al., 2019). With a horizontal resolution of approximately 900 m, the product provides a detailed representation of the long-term thermal conditions in one of the most sensitive fjord-dominated critical zones in the world (Bianchi et al., 2020). To our knowledge, this represents the first high-resolution, multi-decadal in situ-based temperature climatology developed for Northern Patagonia. Previous efforts have provided valuable insights into the regional oceanography through seasonal or annual climatologies derived from shorter time series or satellite products (Saldías et al., 2021; Strub et al., 2019). However, such datasets are generally limited in temporal extent and often too coarse to capture the fine-scale variability inherent to fjord systems. Each subregion of Northern Patagonia responds differently to external forcings such as wind, freshwater discharge, residence time and heat fluxes, all modulated by local topography (Kilpeläinen et al., 2011; Pinilla et al., 2019a, 2021; Soto et al., 2019). Accurately resolving these local variations in temperature is therefore essential to characterise the physical dynamics of the region and understand its sensitivity to environmental change.

The temporal and spatial distribution of the observations is an important consideration when interpreting the climatology. Although the dataset spans 1948–2023, the observations are strongly concentrated in recent decades, with 99 % collected after 1990 and 55 % after 2010. The resulting product should therefore not be interpreted as an equally weighted representation of the mean thermal state over the entire 75-year period. Rather, it primarily reflects the thermal conditions captured by the more densely sampled recent period, while earlier observations provide important historical constraints that extend the climatological reconstruction back to 1948. Consequently, the climatology is best considered a multi-decadal reference field based on observations spanning 1948–2023, rather than a strict baseline of the 75-year period. Spatially, although Comau Fjord accounts for approximately 76 % of the total number of observations due to long-term monitoring efforts, this high sampling density does not imply that the other regions are poorly represented. The main hydrographic regions are all supported by substantial in situ observations, although at considerably lower sampling densities than in Comau Fjord. Moreover, the influence of the particularly dense sampling in Comau Fjord on the reconstructed field is spatially constrained by the 50 km correlation length used in the interpolation, and therefore primarily affects the neighbouring Ancud Gulf rather than the more distant basins. This is further supported by the regional validation, which shows that the different hydrographic regions exhibit distinct

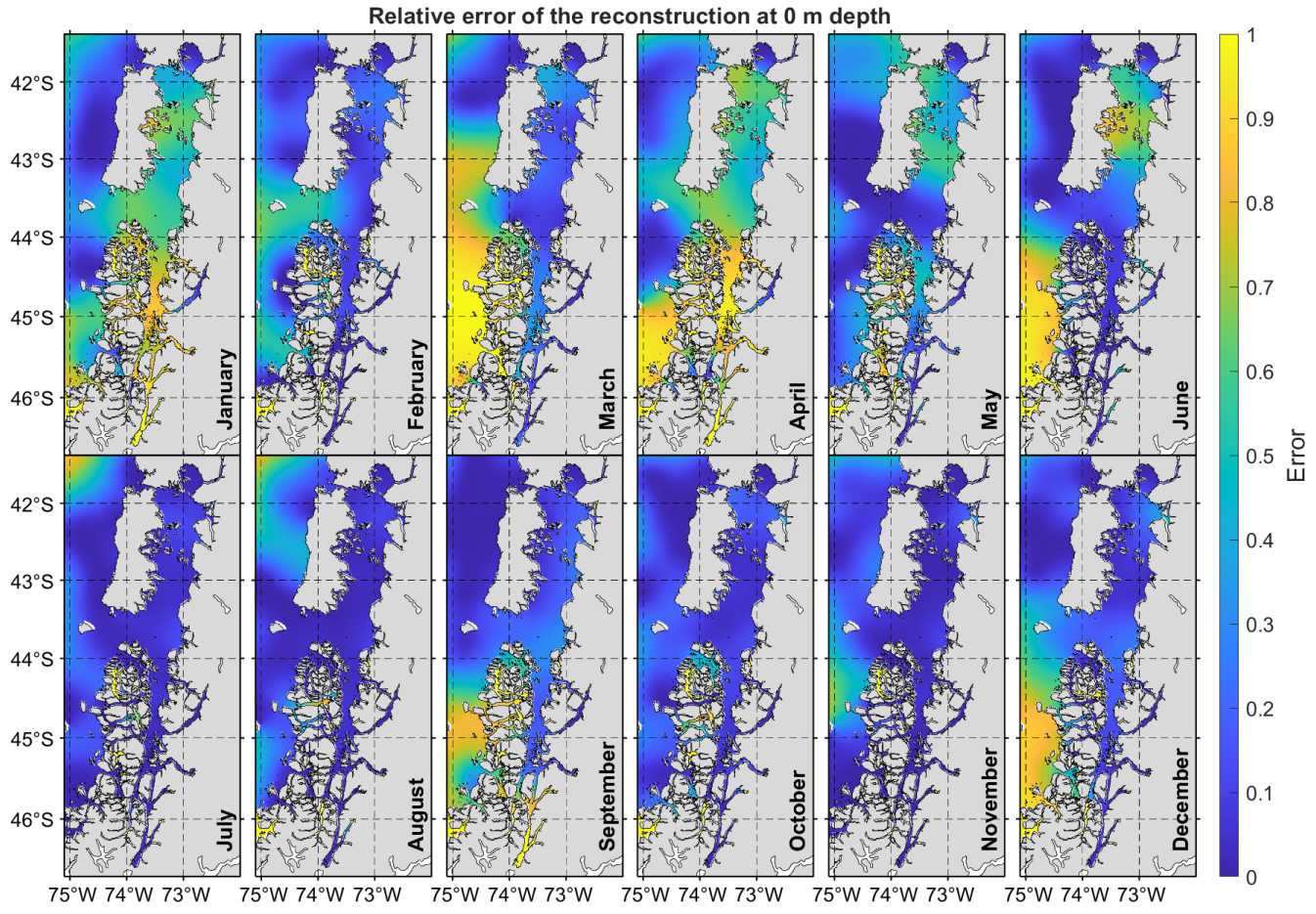


Figure 9. Relative error maps of the climatology at surface.

reconstruction statistics while maintaining overall good performance.

Independent validation was performed at the surface, 30, 100, and 200 m, where the density of observations allowed 5 % of the measurements within the corresponding intervals to be withheld without substantially reducing the data available for the reconstruction. Validation was not extended to greater depths because observations become increasingly sparse with depth, both in number and spatial coverage. Withholding an additional subset of observations at these depths would have further reduced the data available to constrain the interpolation, potentially compromising the reconstruction while providing insufficient independent observations for robust validation. The limitations of validation at depth are illustrated by the 200 m results, for which reliable statistics could not be obtained in January and April because the retained observations did not coincide with locations where the climatology provided interpolated values. We therefore used the DIVAnd relative analysis error fields as an additional diagnostic of the spatial and vertical observational constraint of the climatology rather than as a direct measure of its accuracy. The relative error fields reveal that, despite the heterogeneous sampling of the study region, the fjords and channels of Northern Patagonia are generally well constrained throughout the water column. However, confidence in the reconstruction decreases in poorly sampled regions, such as the Pacific Ocean, as well as during months with sparse observational coverage, such as January. Higher relative error does not necessarily indicate a poor representation of the temperature field, but rather a region where the interpolation relies more on the background field than on the observations. These error fields therefore provide a valuable guide for the appropriate interpretation of the product and identify regions and depths where reconstructed values should be used with greater caution.

Overall, the temperature climatology derived from in situ data in this study shows strong consistency with previous observational and modelling work conducted in Northern Chilean Patagonia. Both the large-scale seasonal cycle and the finer spatial patterns observed at the surface and in subsurface layers closely match those reported in earlier studies (e.g. Castillo et al., 2016; León-Muñoz et al., 2013; Linford et al., 2024; Narváez et al., 2019; Saldías et al., 2021). At the surface, the pronounced west-east gradient detected during

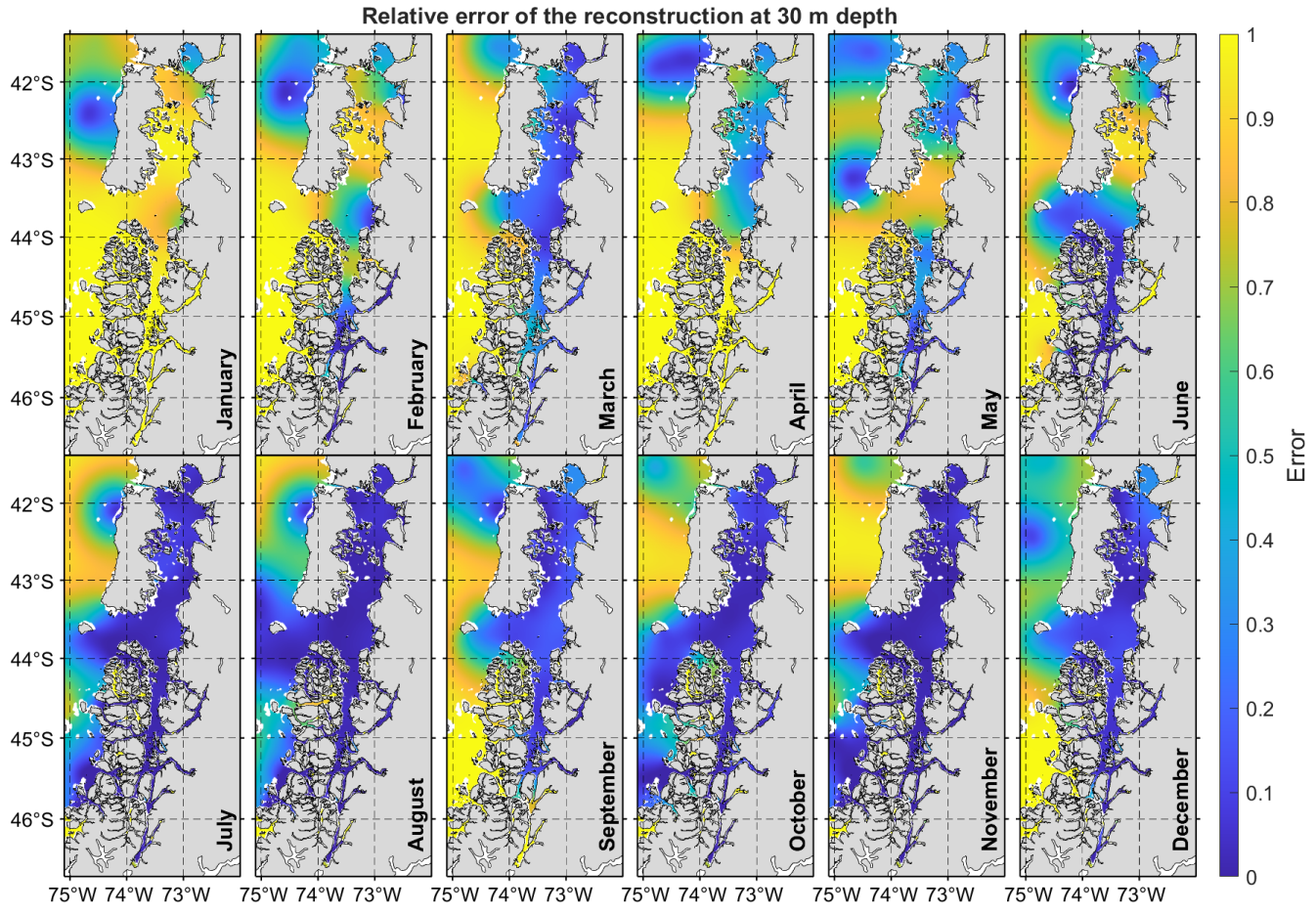


Figure 10. Relative error maps of the climatology at 30 m depth.

summer in both the open ocean and the Inner Sea agrees with satellite and model-based observations (Castillo et al., 2016; León-Muñoz et al., 2013; Linford et al., 2024; Saldías et al., 2021). Similarly, the warm conditions recorded in Reloncaví Sound, Comau Fjord and Puyuhuapi Fjord during summer have been consistently reported in these same studies. The marked contrast between the relatively warm Puyuhuapi Fjord and the cooler Aysén Fjord, despite their close proximity is likely driven by greater freshwater discharge and inputs of glacier meltwater and snowmelt in Aysén (Calvete and Sobarzo, 2011; León-Muñoz et al., 2024; Pinilla et al., 2019b). The colder conditions identified in the Chacao Channel and south of the Desertores Islands are also consistent with Narváez et al. (2019) who attributed these localised minima to tidal mixing and shorter water residence times. The same study also suggested that the higher temperature amplitudes observed in the Inner Sea of Chiloé may be influenced by variations in tidal forcing, local winds and stratification intensity.

The seasonal evolution of surface temperature follows the pattern described by (Saldías et al., 2021), who used 17 years of satellite data to show a strong summer gradient that weakens in autumn, a nearly homogeneous winter distribution (9–12 °C) and renewed warming in spring. The north-south gradient that emerges in austral winter and the relatively cold conditions in Puyuhuapi Fjord (Linford et al., 2024; Pérez-Santos, 2017; Saldías et al., 2021; Schneider et al., 2014) are also captured by the climatology. The higher temperature variability in enclosed fjords such as Reloncaví Sound and the head of Puyuhuapi Fjord agrees with previous findings (Pérez-Santos et al., 2021; Pinilla et al., 2020; Schneider et al., 2014), reflecting the strong influence of freshwater inflows and restricted circulation. Saldías et al. (2021) also showed that the sea surface temperature standard deviation is much higher in enclosed fjords than in more exposed basins (such as Corcovado Gulf), confirming that our interpolation reflects known physical processes. Conversely, open basins such as Corcovado Gulf, Moraleda Channel and Ancud Gulf display smaller seasonal amplitudes, with Corcovado Gulf showing the lowest amplitude, as also noted by Buchan et al. (2021). Narváez et al. (2019) further suggested that the enhanced warming in the northern sector may be partly due to the Desertores Islands, which shelter the surface waters from wind and currents, allowing greater local heating.

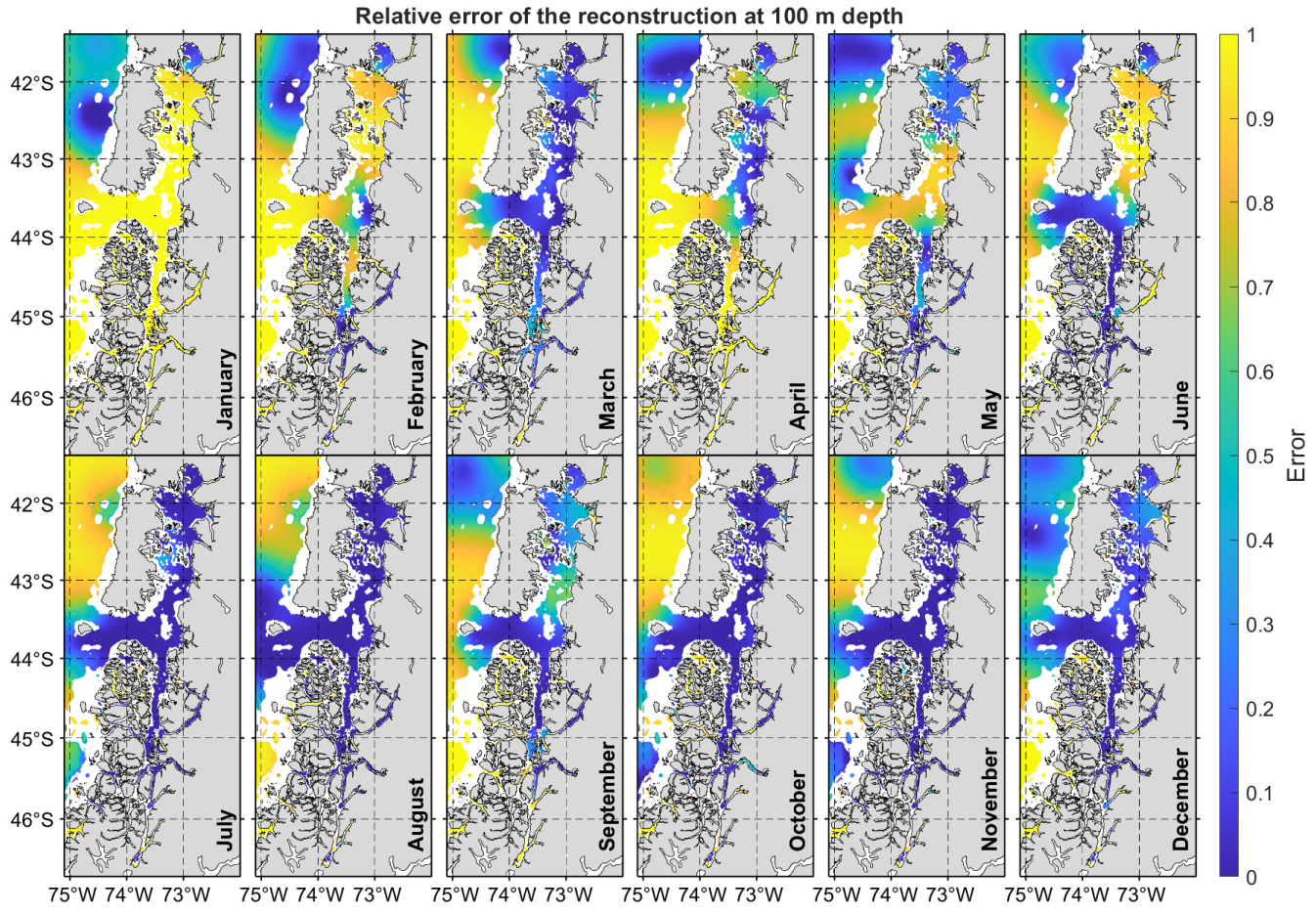


Figure 11. Relative error maps of the climatology at 100 m depth.

Below the surface, the temperature gradually decreases and spatial gradients become smoother, in agreement with observations by Pérez-Santos et al. (2021). At 30 m depth, seasonal variations remain visible, while at 100 m depth, the temperature remains nearly constant throughout the year, although some spatial differences are observed, consistent with results of Pinilla et al. (2021). At 200 m depth, relatively warm conditions persist in the northern basins (Reloncaví Sound and Ancud Gulf) with temperatures around 10 to 11 °C, compared with 8–9 °C in other basins, possibly because the Desertores Islands act as a physical barrier, limiting water renewal and trapping warmer intermediate waters (Linford et al., 2024; Pérez-Santos et al., 2021). At 400 m depth, the temperature stabilises near 7 °C across most of the domain, except in Aysén Fjord, where it fluctuates between 8.5 °C (July to December) and 10 °C (January to June). These seasonal changes likely reflect the long residence time of water in this fjord (up to 120 d; Linford et al., 2024) which buffers rapid thermal adjustments.

The vertical structure provided by the climatology also agrees with previous studies. The thermocline typically develops between the surface and 20 m depth during summer and reaches 50 m in fjords such as Puyuhuapi and Aysén, or in the open ocean west of Chiloé Island. In well-mixed areas such as Guafo Mouth and Corcovado Gulf, the thermocline extends even deeper (up to 100 m) reflecting strong regional vertical mixing (Calvete and Sobarzo, 2011). During winter, the entire water column becomes nearly homogeneous, particularly around Chacao Channel, Ancud Gulf and the northern Corcovado Gulf, as also observed by (Pérez-Santos et al., 2021). The shallow summer mixed layer (typically less than 10 m) and intense surface stratification in fjords and enclosed basins resemble conditions observed in other high-latitude fjords, such as those in Finland (Merkouriadi and Leppäranta, 2015) and Norway (Skogseth et al., 2020). Stratification tends to be stronger at the fjord heads, where freshwater inputs are higher, a pattern also reported for southern Patagonian fjords (Maturana-Martínez et al., 2021) and Arctic fjord systems (Szeligowska et al., 2020).

The climatology developed in this study has a wide range of potential applications in ecological, oceanographic and management contexts. From an ecological perspective, it provides a robust high-resolution reference for assessing thermal niches, predicting shifts in species distributions un-

der climate warming and evaluating the thermal stability of habitats relevant to larval dispersal, or the occurrence of harmful algal blooms (e.g. Aiken et al., 2007; Moore et al., 2008). In the aquaculture sector, the multi-decadal baseline enables comparison between present-day temperatures and historical conditions, helping identify warming hotspots and periods of increased thermal stress for farmed species. The climatology could also support risk mapping for temperature-sensitive species, including the identification of regions with contrasting thermal conditions suitable or not for aquaculture expansion. For environmental monitoring, when combined with near real-time observations from for instance moorings, the climatology provides a reference against which anomalies from expected conditions can be rapidly identified, an approach particularly relevant for managing salmon farming risks associated with harmful algal blooms, oxygen depletion or rapid warming events. Moreover, the monthly and daily-derived fields can serve as an appropriate high-resolution baseline for marine heatwave detection and characterisation, following standard definitions based on long-term climatologies (Hobday et al., 2016). This is especially important in fjord environments, where satellite sea surface temperature products often fail to resolve fine-scale thermal structure. Finally, the climatology can support a wide range of oceanographic applications, including providing a background field for hydrodynamic or biogeochemical models, and serving as a high-resolution reference for model validation in regions where traditional gridded products perform poorly (Lazure et al., 2009; Ridgwell et al., 2007; Vichi et al., 2003).

While the climatology presented here represents a significant advance for the region, several limitations for future improvement should be acknowledged, along with opportunities for future improvement. The observational coverage remains strongly biased towards the surface and certain regions (e.g. Comau Fjord, Reloncaví Sound, Puyuhuapi Fjord), limiting the robustness of the reconstruction in deeper layers and in less-sampled basins. Future updates to the climatology would benefit from the integration of additional data sources, such as aquaculture monitoring stations, which provide high-frequency, multi-depth observations in coastal areas and particularly fjords, where traditional observational platforms, although critically important for understanding local thermal variability, are often scarce. Additionally, the use of a single, domain-wide correlation length (50 km) may not optimally represent the varying spatial scales of different subregions. Future versions could explore regionally varying correlation scales to better capture both fine-scale fjord variability and large-scale open ocean gradients. Finally, as new observations become available, the climatology should be updated periodically to maintain its relevance as a reference for anomaly detection and assessment of long-term changes in this environmentally sensitive region.

6 Code and data availability

The monthly and daily-derived climatologies described in Sects. 2 and 3 are available on Zenodo as NetCDF3-Classic files using geographical coordinates referenced to the WGS84 coordinate reference system under DOI https://doi.org/10.5281/zenodo.21959707 (Pujol et al., 2026) and can be freely used for any purpose. The repository also includes two scripts to facilitate access to and handling of the climatological datasets: a MATLAB script and a Python 3 Jupyter Notebook. These scripts provide examples of how to load, explore and visualise the climatological fields.

Figures fully describing the monthly climatology and the associated relative error maps at every depth level are available in the supplementary material.

The list, description and sources/DOIs of all the in situ data used for the construction of the climatologies (Sect. 2.2) are also available in the Supplement.

7 Conclusions

In this study, a four-dimensional temperature climatology was constructed from approximately 3 million in situ observations collected between 1948 and 2023 in Northern Chilean Patagonia, a region characterised by complex bathymetry, strong freshwater inputs and an extensive network of fjords and channels. This product is a monthly climatology with a horizontal resolution of approximately 900 m and 32 vertical levels from the surface to 400 m. A daily-derived climatology was subsequently generated from the monthly product for the upper 100 m, providing temperature fields at 14 vertical levels and a daily temporal resolution. Together, these products accurately reproduce the long-term thermal conditions of the region and represent, to our knowledge, the first high-resolution, multi-decadal, in situ-based temperature climatology developed for Northern Patagonia. By resolving fjord-scale temperature gradients and identifying distinct spatial and vertical thermal regimes, the climatology provides a refined and physically consistent representation of the oceanographic structure of this highly dynamic region. Enclosed basins such as Reloncaví Sound, Comau and Puyuhuapi Fjords display stronger seasonal temperature amplitudes, while more oceanic systems such as Corcovado Gulf exhibit comparatively more stable conditions.

This approach demonstrates the value of in situ-based reconstructions in regions where satellite observations remain limited by cloud cover and complex coastal geometry. It establishes a robust foundation for future oceanographic analyses and model validation in Northern Chilean Patagonia. The methodology relies exclusively on in situ data, freely accessible online, most of which was collected through local monitoring campaigns funded by public institutions. However, a substantial quantity of high-quality environmental data is also gathered by private operators, particularly aquaculture companies, which routinely monitor temperature, salinity,

oxygen and other parameters at a high temporal frequency. Sharing such data would greatly enhance the spatial and temporal coverage of regional datasets. Closer collaboration and data sharing between the private sector and the scientific community would provide substantial mutual benefits advancing public research while also offering private stakeholders improved environmental knowledge, forecasting capacity and long-term sustainability strategies.

Both climatological products generated in this study are freely available online (Pujol et al., 2026). Together, they provide complementary resources for future scientific research and applied environmental monitoring in Chilean Patagonia.

Supplement. The supplement related to this article is available online at https://doi.org/10.5194/essd-18-8167-2026-supplement.

Author contributions. C.P.: Conceptualization, formal analysis, investigation, methodology, validation, writing (original draft and editing), writing (review and editing). A.B.: Conceptualization, methodology, supervision, validation, writing (original draft and editing), writing (review and editing). I.P-S.: Conceptualization, methodology, resources, supervision, writing (original draft and editing), writing (review and editing). P.L.: Resources, writing (original draft and editing), writing (review and editing). A.A-A.: Conceptualization, methodology, supervision, validation, writing (original draft and editing), writing (review and editing).

Competing interests. The contact author has declared that none of the authors has any competing interests.

Disclaimer. Publisher's note: Copernicus Publications remains neutral with regard to jurisdictional claims made in the text, published maps, institutional affiliations, or any other geographical representation in this paper. The authors bear the ultimate responsibility for providing appropriate place names. Views expressed in the text are those of the authors and do not necessarily reflect the views of the publisher.

Acknowledgements. The authors gratefully acknowledge the Huinay Scientific Field Station for providing openly available online datasets, and the Centro de Investigación i∼mar for providing both free data and material for data collection used in this investigation.

Financial support. This work received financial support from the FRS-FNRS (Fonds de la Recherche Scientifique de Belgique, Communauté Française de Belgique) through funding the position of AB and with a doctoral FRIA grant for CP. IPS was funded by FONDECYT 1251038 and IPS and PL by COPAS COASTAL FB210021.

Review statement. This paper was edited by François G. Schmitt and reviewed by Athanasia Iona and one anonymous referee.

References

Aiken, C., Navarrete, S., Castillo, M., and Castilla, J.: Alongshore larval dispersal kernels in a numerical ocean model of the central Chilean coast, Mar. Ecol. Prog. Ser., 339, 13–24, https://doi.org/10.3354/meps339013, 2007.

Barnier, B., Siefridt, L., and Marchesiello, P.: Thermal forcing for a global ocean circulation model using a three-year climatology of ECMWF analyses, J. Mar. Syst., 6, 363–380, https://doi.org/10.1016/0924-7963(94)00034-9, 1995.

Barth, A., Beckers, J.-M., Troupin, C., Alvera-Azcárate, A., and Vandenbulcke, L.: divand-1.0: n-dimensional variational data analysis for ocean observations, Geosci. Model Dev., 7, 225–241, https://doi.org/10.5194/gmd-7-225-2014, 2014.

Barth, A., Troupin, C., Reyes, E., Alvera-Azcárate, A., Beckers, J.-M., and Tintoré, J.: Variational interpolation of high-frequency radar surface currents using DIVAnd, Ocean Dynam., 71, 293–308, https://doi.org/10.1007/s10236-020-01432-x, 2021.

Beckers, J.-M., Barth, A., Troupin, C., and Alvera-Azcárate, A.: Approximate and Efficient Methods to Assess Error Fields in Spatial Gridding with Data Interpolating Variational Analysis (DIVA), J. Atmos. Ocean. Tech., 31, 515–530, https://doi.org/10.1175/JTECH-D-13-00130.1, 2014.

Bianchi, D., Carozza, D. A., Galbraith, E. D., Guiet, J., and DeVries, T.: Estimating global biomass and biogeochemical cycling of marine fish with and without fishing, Sci. Adv., 7, eabd7554, https://doi.org/10.1126/sciadv.abd7554, 2021.

Bianchi, T. S., Arndt, S., Austin, W. E. N., Benn, D. I., Bertrand, S., Cui, X., Faust, J. C., Koziorowska-Makuch, K., Moy, C. M., Savage, C., Smeaton, C., Smith, R. W., and Syvitski, J.: Fjords as Aquatic Critical Zones (ACZs), Earth-Sci. Rev., 203, 103145, https://doi.org/10.1016/j.earscirev.2020.103145, 2020.

Brasseur, P. P. and Haus, J. A.: Application of a 3-D variational inverse model to the analysis of ecohydrodynamic data in the Northern Bering and Southern Chukchi Seas, J. Mar. Syst., 1, 383–401, https://doi.org/10.1016/0924-7963(91)90006-G, 1991.

Brodie, S., Pozo Buil, M., Welch, H., Bograd, S. J., Hazen, E. L., Santora, J. A., Seary, R., Schroeder, I. D., and Jacox, M. G.: Ecological forecasts for marine resource management during climate extremes, Nat. Commun., 14, 7701, https://doi.org/10.1038/s41467-023-43188-0, 2023.

Buchan, S. J., Pérez-Santos, I., Narváez, D., Castro, L., Stafford, K. M., Baumgartner, M. F., Valle-Levinson, A., Montero, P., Gutiérrez, L., Rojas, C., Daneri, G., and Neira, S.: Intraseasonal variation in southeast Pacific blue whale acoustic presence, zooplankton backscatter, and oceanographic variables on a feeding ground in Northern Chilean Patagonia, Prog. Oceanogr., 199, 102709, https://doi.org/10.1016/j.pocean.2021.102709, 2021.

Calvete, C. and Sobarzo, M.: Quantification of the surface brackish water layer and frontal zones in southern Chilean fjords between Boca del Guafo (43° 30′ S) and Estero Elefantes (46° 30′ S), Cont. Shelf Res., 31, 162–171, https://doi.org/10.1016/j.csr.2010.09.013, 2011.

Castillo, M. I., Cifuentes, U., Pizarro, O., Djurfeldt, L., and Caceres, M.: Seasonal hydrography and surface outflow in a fjord with a

deep sill: the Reloncaví fjord, Chile, Ocean Sci., 12, 533–544, https://doi.org/10.5194/os-12-533-2016, 2016.

Cheng, L. and Zhu, J.: Influences of the Choice of Climatology on Ocean Heat Content Estimation, J. Atmos. Ocean. Tech., 32, 388–394, https://doi.org/10.1175/JTECH-D-14-00169.1, 2015.

Díaz, P. A., Gormaz, R., Aguayo, P., Pérez-Santos, I., Saldías, G. S., Figueroa, R. I., Fernández, P. A., Álvarez, G., Rodríguez-Villegas, C., Schwerter, C., Cassis, D., Vera, R., and Conca, C.: Unveiling the 2017 Karenia Bloom in NW Chilean Patagonia by Integrating Remote Sensing and Field Data, Microorganisms, 13, 2440, https://doi.org/10.3390/microorganisms13112440, 2025.

Dickey, T., Lewis, M., and Chang, G.: Optical oceanography: Recent advances and future directions using global remote sensing and in situ observations, Rev. Geophys., 44, 2003RG000148, https://doi.org/10.1029/2003RG000148, 2006.

Embury, O., Good, S. A., and Merchant, C. J.: ESA Sea Surface Temperature Climate Change Initiative (SST_cci): Climatology Climate Data Record, version 2.2, NERC EDS Centre for Environmental Data Analysis [data set], https://doi.org/10.5285/DC11996A68C446ABB342E917EFDAAC30, 2023.

European Union-Copernicus Marine Service: Global Ocean Physics Reanalysis, Marine Data Store (MDS) [data set], https://doi.org/10.48670/MOI-00021, 2018.

FAO: The State of World Fisheries and Aquaculture 2024, FAO, https://doi.org/10.4060/cd0683en, 2024.

Flaounas, E., Davolio, S., Raveh-Rubin, S., Pantillon, F., Miglietta, M. M., Gaertner, M. A., Hatzaki, M., Homar, V., Khodayar, S., Korres, G., Kotroni, V., Kushta, J., Reale, M., and Ricard, D.: Mediterranean cyclones: current knowledge and open questions on dynamics, prediction, climatology and impacts, Weather Clim. Dynam., 3, 173–208, https://doi.org/10.5194/wcd-3-173-2022, 2022.

Garcia, H. E., Boyer, T. P., Locarnini, R. A., Reagan, J. R., Mishonov, A. V., Baranova, O. K., Paver, C. R., Wang, Z., Bouchard, C., Cross, S., Seidov, D., and Dukhovskoy, D.: World Ocean Database 2023 User's Manual, https://doi.org/10.25923/J8GQ-EE82, 2024.

Goebeler, N., Norkko, A., and Norkko, J.: Ninety years of coastal monitoring reveals baseline and extreme ocean temperatures are increasing off the Finnish coast, Commun. Earth Environ., 3, 215, https://doi.org/10.1038/s43247-022-00545-z, 2022.

Hemming, M. P., Roughan, M., and Schaeffer, A.: Daily Subsurface Ocean Temperature Climatology Using Multiple Data Sources: New Methodology, Front. Mar. Sci., 7, 485, https://doi.org/10.3389/fmars.2020.00485, 2020.

Hobday, A., Alexander, L. V., Perkins, S. E., Smale, D. A., Straub, S. C., Oliver, E. C. J., Benthuysen, J. A., Burrows, M. T., Donat, M. G., Feng, M., Holbrook, N. J., Moore, P. J., Scannell, H. A., Sen Gupta, A., and Wernberg, T.: A hierarchical approach to defining marine heatwaves, Prog. Oceanogr., 141, 227–238, https://doi.org/10.1016/j.pocean.2015.12.014, 2016.

Hoteit, I., Cornuelle, B., Kim, S. Y., Forget, G., Köhl, A., and Terrill, E.: Assessing 4D-VAR for dynamical mapping of coastal high-frequency radar in San Diego, Dyn. Atmos. Oceans, 48, 175–197, https://doi.org/10.1016/j.dynatmoce.2008.11.005, 2009.

Huang, B., Liu, C., Banzon, V., Freeman, E., Graham, G., Hankins, B., Smith, T., and Zhang, H.-M.: Improvements of the Daily Optimum Interpolation Sea Surface Temperature (DOISST) Version 2.1, J. Climate, 34, 2923–2939, https://doi.org/10.1175/JCLI-D-20-0166.1, 2021.

Janjić, T., Bormann, N., Bocquet, M., Carton, J. A., Cohn, S. E., Dance, S. L., Losa, S. N., Nichols, N. K., Potthast, R., Waller, J. A., and Weston, P.: On the representation error in data assimilation, Q. J. Roy. Meteor. Soc., 144, 1257–1278, https://doi.org/10.1002/qj.3130, 2018.

Kilpeläinen, T., Vihma, T., and Ólafsson, H.: Modelling of spatial variability and topographic effects over Arctic fjords in Svalbard, Tellus Dyn. Meteorol. Oceanogr., 63, 223, https://doi.org/10.1111/j.1600-0870.2010.00481.x, 2011.

Lara, C., Saldias, G., Westberry, T., Behrenfeld, M., and Broitman, B.: First assessment of MODIS satellite ocean color products (OC3 and nFLH) in the Inner Sea of Chiloe, northern Patagonia, Lat. Am. J. Aquat. Res., 45, 822–827, https://doi.org/10.3856/vol45-issue4-fulltext-18, 2017.

Lazure, P., Garnier, V., Dumas, F., Herry, C., and Chifflet, M.: Development of a hydrodynamic model of the Bay of Biscay. Validation of hydrology, Cont. Shelf Res., 29, 985–997, https://doi.org/10.1016/j.csr.2008.12.017, 2009.

Legler, D. M., Freeland, H. J., Lumpkin, R., Ball, G., McPhaden, M. J., North, S., Crowley, R., Goni, G. J., Send, U., and Merrifield, M. A.: The current status of the real-time in situ Global Ocean Observing System for operational oceanography, J. Oper. Oceanogr., 8, s189–s200, https://doi.org/10.1080/1755876X.2015.1049883, 2015.

León-Muñoz, J., Marcé, R., and Iriarte, J.: Influence of hydrological regime of an Andean river on salinity, temperature and oxygen in a Patagonia fjord, Chile, N. Z. J. Mar. Freshw. Res., 47, 515–528, https://doi.org/10.1080/00288330.2013.802700, 2013.

León-Muñoz, J., Aguayo, R., Corredor-Acosta, A., Tapia, F. J., Iriarte, J. L., Reid, B., and Soto, D.: Hydrographic shifts in coastal waters reflect climate-driven changes in hydrological regimes across Northwestern Patagonia, Sci. Rep., 14, 20632, https://doi.org/10.1038/s41598-024-71008-y, 2024.

Linford, P., Pérez-Santos, I., Montes, I., Dewitte, B., Buchan, S., Narváez, D., Saldías, G., Pinilla, E., Garreaud, R., Díaz, P., Schwerter, C., Montero, P., Rodríguez-Villegas, C., Cáceres-Soto, M., Mancilla-Gutiérrez, G., and Altamirano, R.: Recent Deoxygenation of Patagonian Fjord Subsurface Waters Connected to the Peru–Chile Undercurrent and Equatorial Subsurface Water Variability, Global Biogeochem. Cy., 37, e2022GB007688, https://doi.org/10.1029/2022GB007688, 2023.

Linford, P., Pérez-Santos, I., Montero, P., Díaz, P. A., Aracena, C., Pinilla, E., Barrera, F., Castillo, M., Alvera-Azcárate, A., Alvarado, M., Soto, G., Pujol, C., Schwerter, C., Arenas-Uribe, S., Navarro, P., Mancilla-Gutiérrez, G., Altamirano, R., San Martín, J., and Soto-Riquelme, C.: Oceanographic processes driving low-oxygen conditions inside Patagonian fjords, Biogeosciences, 21, 1433–1459, https://doi.org/10.5194/bg-21-1433-2024, 2024.

Martínez-Moreno, J., Hogg, A. McC., and England, M. H.: Climatology, Seasonality, and Trends of Spatially Coherent Ocean Eddies, J. Geophys. Res.-Oceans, 127, e2021JC017453, https://doi.org/10.1029/2021JC017453, 2022.

Maturana-Martínez, C., Fernández, C., González, H. E., and Galand, P. E.: Different Active Microbial Communities in Two Contrasted Subantarctic Fjords, Front. Microbiol., 12, 620220, https://doi.org/10.3389/fmicb.2021.620220, 2021.

Merkouriadi, I. and Leppäranta, M.: Influence of sea ice on the seasonal variability of hydrography and heat content in Tvärminne, Gulf of Finland, Ann. Glaciol., 56, 274–284, https://doi.org/10.3189/2015AoG69A003, 2015.

Minnett, P. J., Alvera-Azcárate, A., Chin, T. M., Corlett, G. K., Gentemann, C. L., Karagali, I., Li, X., Marsouin, A., Marullo, S., Maturi, E., Santoleri, R., Saux Picart, S., Steele, M., and Vazquez-Cuervo, J.: Half a century of satellite remote sensing of sea-surface temperature, Remote Sens. Environ., 233, 111366, https://doi.org/10.1016/j.rse.2019.111366, 2019.

Moore, S. K., Trainer, V. L., Mantua, N. J., Parker, M. S., Laws, E. A., Backer, L. C., and Fleming, L. E.: Impacts of climate variability and future climate change on harmful algal blooms and human health, Environ. Health, 7, S4, https://doi.org/10.1186/1476-069X-7-S2-S4, 2008.

Narváez, D. A., Vargas, C. A., Cuevas, L. A., García-Loyola, S. A., Lara, C., Segura, C., Tapia, F. J., and Broitman, B. R.: Dominant scales of subtidal variability in coastal hydrography of the Northern Chilean Patagonia, J. Mar. Syst., 193, 59–73, https://doi.org/10.1016/j.jmarsys.2018.12.008, 2019.

Pantoja, S., Luis Iriarte, J., and Daneri, G.: Oceanography of the Chilean Patagonia, Cont. Shelf Res., 31, 149–153, https://doi.org/10.1016/j.csr.2010.10.013, 2011.

Pérez-Santos, I.: Deep ventilation event during fall and winter 2015 in the Puyuhuapi Fjord (44.6 S), Lat. Am. J. Aquat. Res., 45, 223–227, https://doi.org/10.3856/vol45-issue1-fulltext-25, 2017.

Pérez-Santos, I., Garcés-Vargas, J., Schneider, W., Ross, L., Parra, S., and Valle-Levinson, A.: Double-diffusive layering and mixing in Patagonian fjords, Prog. Oceanogr., 129, 35–49, https://doi.org/10.1016/j.pocean.2014.03.012, 2014.

Pérez-Santos, I., Díaz, P. A., Silva, N., Garreaud, R., Montero, P., Henríquez-Castillo, C., Barrera, F., Linford, P., Amaya, C., Contreras, S., Aracena, C., Pinilla, E., Altamirano, R., Vallejos, L., Pavez, J., and Maulen, J.: Oceanography time series reveals annual asynchrony input between oceanic and estuarine waters in Patagonian fjords, Sci. Total Environ., 798, 149241, https://doi.org/10.1016/j.scitotenv.2021.149241, 2021.

Pinilla, E., Soto, G., Soto-Riquelme, C., Venegas, O., and Salas, P.: Determinación de las escalas de intercambio de agua en fiordos y canales de la Patagonia, Etapa II (Región de Aysén), https://www.researchgate.net/publication/337367262_Determinacion_de_las_escalas_de_intercambio_de_agua_en_fiordos_y_canales_de_la_Patagonia_Etapa_II_Region_de_Aysen (last access: 4 November 2026), 2019a.

Pinilla, E., Soto-Riquelme, C., Soto-Soto, G., San Martín, J., Valdebenito Muñoz, P., and Reche García, P.: Determinación de las escalas de intercambio de agua en fiordos y canales de la Patagonia sur, Etapa II (Región de Aysén), Subsecr. Econ. Empres. Menor Tamaño, https://doi.org/10.13140/RG.2.2.17813.65762, 2019b.

Pinilla, E., Castillo, M. I., Pérez-Santos, I., Venegas, O., and Valle-Levinson, A.: Water age variability in a Patagonian fjord, J. Mar. Syst., 210, 103376, https://doi.org/10.1016/j.jmarsys.2020.103376, 2020.

Pinilla, E., Soto, G., Soto-Riquelme, C., Venegas, O., Salas, P., and Cortés, J.: Determinación de las escalas de intercambio de agua en fiordos y canales de la región de Los Lagos y región de Aysén, Subsecr. Econ. Empres. Menor Tamaño, https://doi.org/10.13140/RG.2.2.17813.65762, 2021.

Pujol, C., Barth, A., Pérez-Santos, I., Linford, P., and Alvera-Azcárate, A.: Climatology (Daily and Monthly) of the Sea Temperature in the Chilean Northern Patagonia, Zenodo [data set], https://doi.org/10.5281/zenodo.21959707, 2026.

Ridgwell, A., Hargreaves, J. C., Edwards, N. R., Annan, J. D., Lenton, T. M., Marsh, R., Yool, A., and Watson, A.: Marine geochemical data assimilation in an efficient Earth System Model of global biogeochemical cycling, Biogeosciences, 4, 87–104, https://doi.org/10.5194/bg-4-87-2007, 2007.

Rodrigo, C.: Submarine topography in the Chilean North Patagonian channels, in: Progress in the oceanographic knowledge of Chilean inner waters, from Puerto Montt to Cape Horn, 19–23, 2008.

Saldías, G. S., Sobarzo, M., and Quiñones, R.: Freshwater structure and its seasonal variability off western Patagonia, Prog. Oceanogr., 174, 143–153, https://doi.org/10.1016/j.pocean.2018.10.014, 2019.

Saldías, G. S., Hernández, W., Lara, C., Muñoz, R., Rojas, C., Vásquez, S., Pérez-Santos, I., and Soto-Mardones, L.: Seasonal Variability of SST Fronts in the Inner Sea of Chiloé and Its Adjacent Coastal Ocean, Northern Patagonia, Remote Sens., 13, 181, https://doi.org/10.3390/rs13020181, 2021.

Schneider, W., Pérez-Santos, I., Ross, L., Bravo, L., Seguel, R., and Hernández, F.: On the hydrography of Puyuhuapi Channel, Chilean Patagonia, Prog. Oceanogr., 129, 8–18, https://doi.org/10.1016/j.pocean.2014.03.007, 2014.

Senay, G. B., Parrish, G. E. L., Schauer, M., Friedrichs, M., Khand, K., Boiko, O., Kagone, S., Dittmeier, R., Arab, S., and Ji, L.: Improving the Operational Simplified Surface Energy Balance Evapotranspiration Model Using the Forcing and Normalizing Operation, Remote Sens., 15, 260, https://doi.org/10.3390/rs15010260, 2023.

Shahzadi, K., Pinardi, N., Barth, A., Troupin, C., Lyubartsev, V., and Simoncelli, S.: A New Global Ocean Climatology, Front. Environ. Sci., 9, 711363, https://doi.org/10.3389/fenvs.2021.711363, 2021a.

Shahzadi, K., Zavatarelli, M., and Pinardi, N.: SeaDataCloud Dissolved Oxygen and Apparent Oxygen Utilization Climatology for the Global Ocean, SeaDataCloud, https://doi.org/10.13155/79295, 2021b.

Sievers, H. and Silva, N.: Water masses and circulation in austral Chilean channels, in: Progress in the oceanographic knowledge of Chilean inner waters, from Puerto Montt to Cape Horn, 53–58, 2008.

Simoncelli, S., Oliveri, P., and Mattia, G.: SeaDataCloud Temperature and Salinity Climatology for the Mediterranean Sea (Version 1), SeaDataCloud, https://doi.org/10.13155/77506, 2020.

Skogseth, R., Olivier, L. L. A., Nilsen, F., Falck, E., Fraser, N., Tverberg, V., Ledang, A. B., Vader, A., Jonassen, M. O., Søreide, J., Cottier, F., Berge, J., Ivanov, B. V., and Falk-Petersen, S.: Variability and decadal trends in the Isfjorden (Svalbard) ocean climate and circulation – An indicator for climate change in the European Arctic, Prog. Oceanogr., 187, 102394, https://doi.org/10.1016/j.pocean.2020.102394, 2020.

Soto, D., León-Muñoz, J., Dresdner, J., Luengo, C., Tapia, F. J., and Garreaud, R.: Salmon farming vulnerability to climate change in southern Chile: understanding the biophysical, socioeconomic and governance links, Rev. Aquac., 11, 354–374, https://doi.org/10.1111/raq.12336, 2019.

Soto-Riquelme, C., Pinilla, E., and Ross, L.: Wind influence on residual circulation in Patagonian channels and fjords, Cont. Shelf Res., 254, 104905, https://doi.org/10.1016/j.csr.2022.104905, 2023.

Strub, P. T., James, C., Montecino, V., Rutllant, J. A., and Blanco, J. L.: Ocean circulation along the southern Chile transition region (38–46° S): Mean, seasonal and interannual variability, with a focus on 2014–2016, Prog. Oceanogr., 172, 159–198, https://doi.org/10.1016/j.pocean.2019.01.004, 2019.

Subsecretaría del Trabajo, Gobierno de Chile and Observatorio Laboral de la Región de Aysén: EQUIPO OBSERVATORIO LABORAL AYSÉN, 2024.

Szeligowska, M., Trudnowska, E., Boehnke, R., Dąbrowska, A. M., Wiktor, J. M., Sagan, S., and Błachowiak-Samołyk, K.: Spatial Patterns of Particles and Plankton in the Warming Arctic Fjord (Isfjorden, West Spitsbergen) in Seven Consecutive Mid-Summers (2013–2019), Front. Mar. Sci., 7, 584, https://doi.org/10.3389/fmars.2020.00584, 2020.

Troupin, C., Machín, F., Ouberdous, M., Sirjacobs, D., Barth, A., and Beckers, J.-M.: High-resolution climatology of the northeast Atlantic using Data-Interpolating Variational Analysis (Diva), J. Geophys. Res.-Oceans, 115, 2009JC005512, https://doi.org/10.1029/2009JC005512, 2010.

Troupin, C., Barth, A., Sirjacobs, D., Ouberdous, M., Brankart, J.-M., Brasseur, P., Rixen, M., Alvera-Azcárate, A., Belounis, M., Capet, A., Lenartz, F., Toussaint, M.-E., and Beckers, J.-M.: Generation of analysis and consistent error fields using the Data Interpolating Variational Analysis (DIVA), Ocean Model., 52–53, 90–101, https://doi.org/10.1016/j.ocemod.2012.05.002, 2012.

Vásquez, S. I., De La Torre, M. B., Saldías, G. S., and Montecinos, A.: Meridional Changes in Satellite Chlorophyll and Fluorescence in Optically-Complex Coastal Waters of Northern Patagonia, Remote Sens., 13, 1026, https://doi.org/10.3390/rs13051026, 2021.

Vichi, M., Oddo, P., Zavatarelli, M., Coluccelli, A., Coppini, G., Celio, M., Fonda Umani, S., and Pinardi, N.: Calibration and validation of a one-dimensional complex marine biogeochemical flux model in different areas of the northern Adriatic shelf, Ann. Geophys., 21, 413–436, https://doi.org/10.5194/angeo-21-413-2003, 2003.

WMO: Guide to Climatological Practices, World Meteorological Organization, Geneva, Switzerland, ISBN 978-92-63-10100-6, 2023.